BASIC RESEARCH www.jasn.org

Complementary Nck1/2 Signaling in Podocytes Controls α Actinin-4–Mediated Actin Organization, Adhesion, and Basement Membrane Composition

Claire E. Martin,[1,2] Noah J. Phippen,[1] Ava Keyvani Chahi,[1,3] Manali Tilak,[1] Sara L. Banerjee,[4,5] Peihua Lu,[1] Laura A. New,[1] Casey R. Williamson,[1] Mathew J. Platt,[6] Jeremy A. Simpson,[6] Mira Krendel,[7] Nicolas Bisson,[4,5,8] Anne-Claude Gingras,[2,9] and Nina Jones[1]

Due to the number of contributing authors, the affiliations are listed at the end of this article.

ABSTRACT

Background Maintenance of the kidney filtration barrier requires coordinated interactions between podocytes and the underlying glomerular basement membrane (GBM). GBM ligands bind podocyte integrins, which triggers actin-based signaling events critical for adhesion. Nck1/2 adaptors have emerged as essential regulators of podocyte cytoskeletal dynamics. However, the precise signaling mechanisms mediated by Nck1/2 adaptors in podocytes remain to be fully elucidated.

Methods We generated podocytes deficient in Nck1 and Nck2 and used transcriptomic approaches to profile expression differences. Proteomic techniques identified specific binding partners for Nck1 and Nck2 in podocytes. We used cultured podocytes and mice deficient in Nck1 and/or Nck2, along with podocyte injury models, to comprehensively verify our findings.

Results Compound loss of Nck1/2 altered expression of genes involved in actin binding, cell adhesion, and extracellular matrix composition. Accordingly, Nck1/2-deficient podocytes showed defects in actin organization and cell adhesion *in vitro*, with podocyte detachment and altered GBM morphology present *in vivo*. We identified distinct interactomes for Nck1 and Nck2 and uncovered a mechanism by which Nck1 and Nck2 cooperate to regulate actin bundling at focal adhesions *via* α actinin-4. Furthermore, loss of Nck1 or Nck2 resulted in increased matrix deposition *in vivo*, with more prominent defects in Nck2-deficient mice, consistent with enhanced susceptibility to podocyte injury.

Conclusion These findings reveal distinct, yet complementary, roles for Nck proteins in regulating podocyte adhesion, controlling GBM composition, and sustaining filtration barrier integrity.

JASN 33: 1546–1567, 2022. doi: https://doi.org/10.1681/ASN.2021101343

The glomerular filtration barrier consists of fenestrated endothelium, the glomerular basement membrane (GBM) and "foot" processes of specialized epithelial cells, termed podocytes.[1] Foot processes are actin-rich terminal projections that interdigitate to encapsulate the glomerular vasculature. They attach to the underlying GBM *via* $\alpha 3\beta 1$-integrin–containing adhesions[2,3] and to each other *via* unique cell-cell junctions, termed slit diaphragms.[4] This network of podocyte adhesions creates a lattice that contributes to filtration selectivity by providing tension to counteract the pressure of fluid flow across the GBM.[5] Disruption of either the podocyte's actin cytoskeleton,

Received October 15, 2021. Accepted April 26, 2022.

Published online ahead of print. Publication date available at www.jasn.org.

Correspondence: Dr. Nina Jones, Department of Molecular and Cellular Biology, University of Guelph, 50 Stone Road East, Room 3461, Summerlee Science Complex, Guelph, ON N1G 2W1, Canada. Email: jonesmcb@uoguelph.ca

its adhesive components, or the connections between them leads to foot process retraction, often accompanied by podocyte detachment. In turn, this triggers failure of the filtration barrier, leading to loss of blood proteins into the urine (proteinuria), and, ultimately, the development of kidney disease.[1,4]

Bidirectional communication between the extracellular matrix (ECM) and the podocyte's cytoskeletal framework is permitted *via* integrin-based adhesions. Despite recent efforts to identify the componentry of the podocyte adhesome[6] and that of the specialized GBM to which they are linked,[7] how podocytes remain adherent in the face of the immense mechanophysical strain of the glomerular vasculature is not well understood. The cytoplasmic tail of active β1-integrin binds several anchoring proteins, including α actinin-4.[8] Various mutations in the α actinin-4–coding gene, *ACTN4*, have been identified in patients with FSGS, and each of these targets its actin-binding domain, increasing its binding affinity to filamentous actin (F-actin). This results in abnormal, actin-rich cellular aggregates[9] and maladaptation to physical forces at β1-integrin–based adhesions.[10] Emerging evidence suggests that actin recruitment to integrin adhesions by α actinin-4 is not only central to their force-dependent maturation but also in shaping ECM deposition within the GBM.[11] These findings suggest an intimate relationship between the podocyte's contractile actin cytoskeleton, integrin adhesions, and the underlying GBM, although the mechanisms governing these associations are largely unexplored.

The Nck family of cytoskeletal adaptors, made up of the structurally similar paralogs Nck1 and Nck2, orchestrate Arp2/3-dependent actin nucleation *via* their association with N-WASp.[12,13] Collectively, Nck proteins are essential for establishment of podocyte foot processes during development[13,14] and for their preservation throughout adulthood.[15] However, the precise signaling mechanisms underlying their essentiality within podocytes are unclear, and the individual and/or redundant functions of each paralog have yet to be defined. We now reveal previously unidentified functions for Nck1 and Nck2 in influencing the composition of and adhesion to the podocyte GBM. Furthermore, we provide molecular insights to explain their pivotal contributions to cytoskeletal stabilization at focal adhesions. Together, these results point to multifaceted and complementary coordination between Nck1 and Nck2 in regulating podocyte foot process structure, adhesion, and filtration barrier integrity at both the level of gene expression and protein complex formation.

Significance Statement

Podocyte detachment is a major contributor to kidney disease progression, yet the mechanisms controlling podocyte adhesion are not well understood. We identified novel roles for Nck1 and Nck2 cytoskeletal adaptor proteins in cell adhesion through regulation of actin bundling at focal adhesions *via* α actinin-4. *In vivo*, loss of Nck1 and/or Nck2 increases basement membrane matrix deposition and renders podocytes more susceptible to damage after injury and with aging. More severe defects are observed with Nck2 deficiency, consistent with identification of distinct effector proteins. The results suggest an essential role for Nck adaptors as molecular hubs integrating multiple actin-based signals to control podocyte adhesion dynamics.

METHODS

Cell Line Generation and Culture Conditions

Mouse podocyte cells (MPCs) were generated by isolating podocytes from Immortomouse (catalog number 238, official designation CBA;B10-Tg[H2Kb-tsA58]6Kio/Crl; Charles River) mice crossed to appropriate Nck transgenic mice (Supplemental Figure 1A) according to standardized protocols.[16] Type 5 recombinant adenoviruses (Vector Biolabs), in which E1 and E3 were deleted, were used to express Cre recombinase or green fluorescent protein, producing double knockout (dKO) and wild-type (WT) lines. An moi of 500 was used for MPCs, and no detectable toxicity was observed. Knockout (KO) efficiency in the resultant pool of cells was confirmed using RT-PCR (Supplemental Figure 1B) and Western immunoblotting for Nck (Supplemental Figure 1C). Cells were grown under permissive conditions in DMEF/12 (Hyclone) with 10% FBS, 200 U/ml penicillin, 200 μg/ml streptomycin (Invitrogen), and 20 U IFN-γ (Peprotech) at 33°C and 5% carbon dioxide (CO_2), and then thermoswitched to 37°C with 2% FBS-containing medium for 10–14 days to induce differentiation (Supplemental Figure 1D). Cell lines were tested regularly for the presence of *Mycoplasma*.

Microarray

RNA was isolated from snap-frozen cell pellets using Trizol and integrity was verified after DNAse treatment on a bioanalyzer (Agilent Technologies, Santa Clara, CA); all samples used for analysis had a RIN value of ten. Samples ($n=3$) were further processed by the Microarray Facility at the Centre for Applied Genomics (The Hospital for Sick Children). Briefly, 5.5 μg of cDNA was labeled with biotin allonamide triphosphate, hybridized for 16 hours at 45°C, and analyzed on an Affymetrix GeneChip MTA 1.0 MTA1 array plate (Affymetrix, Santa Clara, CA) using an Affymetrix GeneChip Scanner 3000. Raw data were preprocessed by using the three-step function from the affyPLM package (version 1.42.0), using default values: background correction method=RMA.2 (RMA convolution background model), normalization method=quantile, summarization method=median polish. Given the numeric range of the output, the data appeared to be normalized when log2 transformed, as confirmed by visually comparing the box plots of raw and processed data (Supplemental Figure 2A). The dataset had 72,688 transcripts. Linear models were applied to assess the statistical significance of differential expression in R using limma. To eliminate false positives

and increase data accuracy and quality, the Bonferroni method for correction was used to correct *P* values derived from the limma algorithm. A confidence level of 95% was used as a cutoff for statistical significance, yielding differentially expressed genes (3764 upregulated, 4304 downregulated). Fold-change analysis was also conducted on this reduced data to obtain two-fold up- and downregulated genes (243 upregulated, 158 downregulated). For Gene Ontology (GO) analysis, up- and downregulated gene lists were analyzed separately using the gost function in *gprofiler2* (version 0.2.0) R package with the following parameters: organism="mmusculus," ordered_query=TRUE, evcodes=TRUE, sources="GO." A custom background made up of the mouse microarray gene list was used, electronic annotations were not considered, and only terms with <500 genes were used. Next, relative abundances for terms that were enriched in both up- and downregulated clusters were calculated on the basis of the number of intersecting genes (counts) for each cluster using the *make relative* function from the *funrar* (version 1.4.1) R package. Dot plots were generated using the *ggplot2* (version 3.3.5) R package and organized manually into biologic themes for clarity. A complete list of GO terms called can be found in Supplemental Figure 3.

For gene set enrichment analysis (GSEA), first a ranked list of differentially expressed genes from the microarray was created by sorting the gene list according to fold changes in descending order. Background gene sets were retrieved using the *msigdbr* (version 7.4.1) package with the following settings: species="mus musculus" and category="C5" (representing GO gene set collection). Next, R package *clusterProfiler* (3.18.1) was used to perform GSEA on the ranked list using the following parameters: minGSSize=2, maxGSSize=500, and *P*valueCutoff=0.05. Normalized enrichment scores were obtained, and terms with a *q* value <0.05 were considered enriched. An enrichment map of GSEA findings was generated using *EnrichmentMap* in Cytoscape, allowing for the collapse of redundant pathways into a singular biologic theme. *AutoAnnotate* was used to automatically find and collapse nodes further into clusters and to visually annotate them within the map, which was manually reorganized for clarity. Finally, a dot plot of normalized enrichment scores against enriched terms was generated using the *ggplot2* (version 3.3.5) R package. Microarray data have been made available in the Gene Expression Omnibus (GEO) repository (https://www.ncbi.nlm.nih.gov/geo) as accession GSE184235.

Cell Lysis

Cells were placed on ice and lysed in cold PLC+ lysis buffer (PLC+; 50 mM HEPES, pH 7.5, 150 mM sodium chloride [NaCl], 10% glycerol, 1% Triton X-100, 15 mM magnesium chloride, 1 mM EGTA, 10 mM NaPPi, 100 mM sodium fluoride [NaF]) supplemented with fresh protease and phosphatase inhibitors (1 mM PMSF, 1 mM sodium orthovanadate, 10 μg/ml aprotinin, and 10 μg/ml leupeptin) and snap frozen at −80°C. Passive lysis (quick thaw and nutation at 4°C for 30 minutes) was followed by centrifuging at 16,000 × *g* for 20 minutes at 4°C. Protein concentrations in supernatants were determined using a bicinchoninic acid (BCA) Protein Assay (Pierce, Rockford, IL). Supernatants were mixed with appropriate amounts of SDS sample buffer and incubated at 100°C for 5 minutes.

Glomerular Isolations and Lysis

Glomeruli were isolated from mice, as described previously,[17] and lysed in cold PLC lysis buffer (10% glycerol, 50 mM HEPES, 150 mM NaCl, 1.5 mM magnesium chloride, 1 mM EGTA, 10 mM NaPPi, 100 mM NaF, and 1% Triton X-100) supplemented with fresh inhibitors, sonicated for 10 seconds on ice, incubated on ice for 5 minutes, and then centrifuged at 14,000 × *g* for 10 minutes at 4°C. Protein concentrations were determined using a BCA Protein Assay. Supernatants were mixed with appropriate amounts of 5× SDS sample buffer and incubated at 100°C for 5 minutes.

Adenoviral Transductions

The AdEasy XL Adenoviral System (Agilent Technologies) was used to generate mCherry-paxillin, FLAG-hNCK1, FLAG-hNCK2, and FLAG (control) viruses,[18] which were collectively used for live-cell imaging, rescue, and affinity purification–mass spectrometry (AP-MS) experiments. Differentiated MPCs were infected with the indicated viruses at a dilution of 1:100 in 2% FBS-containing DMEF/12 over 16–36 hours.

Coimmunoprecipitations

For immunoprecipitation of endogenous Nck, α actinin-4, or rabbit IgG (control), 1 μl of antibody was mixed with 100 μl protein A beads (Invitrogen). Glomerular lysate (2 mg) or 300 μl of cell lysate were incubated for 4 hours at 4°C with rotation. For immunoprecipitation of FLAG, cleared lysates were incubated with FLAG-M2 agarose beads (Sigma-Aldrich, St. Louis, MO) for 4 hours at 4°C with rotation. After three successive washes in PLC+, immunoprecipitated proteins were eluted in 100 μl of 2× SDS with boiling for 5 minutes at 100°C. Antibody information can be found in Supplemental Table 1.

Immunoblotting

Protein samples were resolved on 10% SDS-PAGE gels with 10–20 μg protein loaded as total lysate, or 1:10 of immunoprecipitated samples. Proteins were transferred to polyvinylidene difluoride membrane (EMD Millipore, Billerica, MA) and blocked in 5% BSA in 1× Tris-buffered saline/Tween 20. Membranes were incubated with primary antibodies (Supplemental Table 2) overnight at 4°C. Signals were detected using ECL (Pierce) or Luminata Crescendo (EMD Millipore). Blots were imaged using a ChemiDoc XRS+ (Bio-Rad) or

exposed to film (Pierce). Densitometry was performed using *ImageLab* version 2.0 analysis software (Bio-Rad).

Immunofluorescence Microscopy

For immunofluorescence of cultured podocytes, cells were differentiated on collagen IV–coated coverslips for 10 days before fixing in 4% paraformaldehyde (PFA) for 10 minutes and permeabilization in 0.1% Triton X-100 for 10 minutes. After blocking for 1 hour in 2.5% milk, slides were incubated in primary antibody for 1 hour (Supplemental Table 3), washed three times in PBS, and incubated with secondary antibody (plus phalloidin) for an additional 1 hour. After thorough washing, slides were mounted in Prolong Gold Antifade Mounting Medium (Invitrogen). Epifluorescence images were obtained using *Volocity* software version 5.3.2 (Improvision) on a DMIRE2 microscope (Leica Microsystems) using the 20× or 40× objective.

For immunofluorescence of kidney samples, cortex segments were flash frozen in Cryomatrix (Fisher Scientific, Waltham, MA); 6-μm sections were dried at room temperature for 10 minutes, fixed, and permeabilized in acetone at −20°C for 10 minutes. All subsequent steps were carried out at room temperature. Slides were blocked for 1 hour in 10% goat serum and then incubated with primary antibodies for 1 hour (Supplemental Table 3). After three washes in PBS, slides were incubated with secondary antibodies for 1 hour (goat anti-rabbit Alexa 488 and goat anti–guinea pig Alexa 594; both 1:400). Slides were washed and mounted using Prolong Gold Antifade Mounting Medium (Invitrogen). Epifluorescence images were obtained using *Volocity* software version 5.3.2 (Improvision) on a DMIRE2 Microscope (Leica Microsystems) using the 40× objective. Stacks were captured at 0.2-μm z intervals and then deconvolved using an iterative restoration function (95% CI with 15 iterations) in *Volocity*.

Confocal Live-Cell Microscopy

Podocytes were differentiated on Mattek tissue culture plates coated with type IV collagen and transduced with paxillin-mCherry adenovirus at a dilution of 1:1000 in 2% FBS-containing DMEF/12 16 hours before imaging. After 5 minutes of equilibration in an environmental chamber, cells were imaged at 37°C using a PerkinElmer (Waltham, MA) UltraView VoX Spinning Disk Confocal Imaging System mounted on a Nikon Eclipse Ti-E microscope equipped with Hamamatsu C9100-50 EMCCD camera and a 100×/1.4 N.A. PlanApo objective, controlled by *Volocity* software. Time series were collected at 1 minute intervals for 22 minutes.

Quantification of Actin and Focal Adhesion Characteristics

In Fiji, 60× magnification images of paxillin (focal adhesions) and phalloidin (F-actin) from three independent experiments were converted to 8-bit binary images. To quantify focal adhesion number and size, the "analyze particles" command was used (size parameter=50–infinity and circularity=0.00–0.99). The *Ridge (Line) Detection* plugin was used to quantify F-actin length and width.

Wound Closure Cell Migration Assay

For the wound closure assay, MPCs were plated on type IV collagen–coated coverslips and allowed to differentiate for 10 days in 2% serum. On day 11, cultures were wounded in a crosslike manner with a sterile micropipette tip, and 10% serum-containing medium was added. Cultures were imaged at consistent locations at 1 hour (baseline) and 48 hours. Images were acquired using a Leica DMIRE2 microscope and Leica CTR MIC camera.

Cell Adhesion and Spreading Assays

Differentiated podocytes were trypsinized and plated on type IV collagen–coated coverslips in medium supplemented with 10% FBS, 100 U/ml penicillin, and 50 μg/ml streptomycin. Slides were fixed in 4% (vol/vol) PFA in PBS for 10 minutes at room temperature at the indicated time points. Samples were then fluorescently immunostained with Texas Red phalloidin (1:40; Invitrogen), and paxillin (1:50; Santa Cruz) in PBS and mounted in ProLong Gold mounting medium with 4′,6-diamidino-2-phenylindole (Invitrogen). Samples were observed under a Leica DMIRE2 epifluorescence microscope, and the numbers of adherent cells were quantified by counting nuclei positive for 4′,6-diamidino-2-phenylindole in 20 random fields at 20× optical zoom. Cell surface area was quantified after staining with phalloidin in *Volocity*'s measurement module (at least 30 cells for each replicate). A lower limit of zero was used for the SD of illumination intensity, and objects <500 μm^3, or those that touched the edge of the imaging area, were excluded. The "separate touching objects" function was set to 1500 μm^3. Quantifications were automated and monitored thereafter to ensure accuracy.

Actin Sedimentation Assay

The content of F-actin versus free globular actin (G-actin) was determined in WT and dKO cells using the G-Actin/F-Actin *In Vivo* Assay (BK037; Cytoskeleton, Inc.) as per the manufacturer's instructions. Briefly, differentiated podocytes were homogenized in F-actin stabilization buffer, followed by centrifugation to separate the F-actin from the G-actin pool. The fractions were resolved by SDS-PAGE and the proportions of actin and α actinin-4 were visualized in each fraction by Western blot (representative results from three independent experiments shown).

CRISPR

CRISPR single-guide RNA (sgRNA) guides (Supplemental Table 4) were designed at benchling.com using an optimal available combination of on-target and off-target scores.

Guides were subcloned using type IIs restriction cloning into the pSpCas9(BB)-2A-Puro (PX459) V2.0 plasmid (plasmid number 62988; Addgene[19]).

MPC cells plated in six-well plates were transfected with 1–2 μg PX459v2.0 plasmid containing the desired sgRNA using lipofectamine 3000 (as per manufacturer's indications). At 18 hours after transfection, puromycin (WT MPCs, 2 μg/ml; dKO MPCs, 3 μg/ml) was added to the media. Exchange with fresh puromycin-containing media was repeated for a further 48 hours to eliminate untransfected cells. Media was then changed to fresh (puromycin-free) media during cell recovery and expansion. Pooled KO cell populations were confirmed by Western immunoblotting and tracking of indels by decomposition (TIDE) analysis before use in subsequent experiments.

TIDE Analysis

For pooled KO lines, the efficiency of genomic target disruption was assessed by TIDE analysis.[20] Genomic DNA was isolated from pooled KO lines using GenElute Genomic DNA Purification Kit (Sigma), and regions flanking the guide sequence were amplified by PCR (Supplemental Table 4). PCR products were purified by gel extraction using the Purelink Gel Extraction kit (Invitrogen), subjected to Sanger sequencing, and the efficiency of gene disruption relative to the scrambled KO condition was determined using the TIDE web tool (tide.nki.nl). The proportion of DNA with frameshifting indels is listed as a percentage value in Supplemental Table 4. Attempts to amplify the *Lima1* gene target were unsuccessful, therefore, Western immunoblotting was used to evaluate depletion.

AP-MS

FLAG-NCK1, FLAG-NCK2, or -FLAG (control) adenoviruses were used to infect WT MPCs on day 10–12 of differentiation. Cells were harvested 36 hours later by scraping in AP-MS lysis buffer (20-mM Tris-HCl, pH 7.4, 150-mM NaCl, 1-mM EDTA, 1% nonidet P-40, 0.5% sodium deoxycholate, 10-mM β-glycerophosphate, 10-mM sodium pyrophosphate, 50-mM NaF, 10% glycerol) supplemented with protease inhibitors (1-mM PMSF, 10-μg/ml aprotinin, 10-μg/ml leupeptin, 10-μg/ml pepstatin) and phosphatase inhibitors (Cocktail 2; Sigma-Aldrich) and snap frozen on dry ice before sample processing. Each replicate consisted of three 15-cm plates of cells, independently differentiated and pooled at lysis. FLAG affinity purification experiments were performed as previously described.[21] Briefly, cleared supernatants were incubated with FLAG-M2 agarose beads (Sigma-Aldrich) for 2 hours at 4°C with rotation. Beads were washed three times with lysis buffer, followed by two washes with 20-mM Tris-HCl (pH 7.4). For mass spectrometry, proteins were eluted three times with 50-mM phosphoric acid for 10 minutes and stored at −80°C. Eluted proteins were digested with Promega Sequencing Grade Modified Trypsin (Thermo Fisher Scientific) as described previously.[22] The resulting peptides were desalted using StageTips[23] and dried down by vacuum centrifugation.

Mass Spectrometry Acquisition and Analysis

Each sample (6 μl in 2% formic acid; corresponding to a third of three pooled 15-cm tissue culture dishes) was directly loaded at 800 nl/min onto an equilibrated high-performance liquid chromatography column and liquid chromatography tandem mass spectrometry was performed on a TripleTOF instrument as previously reported.[24] Samples were analyzed with two separate injections with instrument methods set to data-dependent acquisition and data-independent acquisition (DIA; also known as SWATH) modes, as reported previously.[24] Briefly, DIA mass spectrometry data were analyzed using *MSPLIT-DIA* (version 1.0[25]) implemented in *ProHits 4.0*,[26] and spectral counting was used for a semiquantitative assessment. To generate a sample-specific spectral library, peptide-spectrum matches from matched data-dependent acquisition runs were pooled by retaining only the spectrum with the best MS-GFDB (β version 1.0072; June 30, 2014[27]) probability for each unique peptide sequence and precursor charge state, and a peptide-level false discovery rate (FDR) of 1% was enforced using a target-decoy approach.[28] The MS-GFDB parameters were set to search for tryptic cleavages with a precursor mass tolerance of 50 ppm and charges of 2+ to 4+. Peptide length was limited to 8–30 amino acids and oxidized methionine selected as a variable modification. The spectra were searched using the National Center for Biotechnology Information RefSeq database (version 57; January 30, 2013) against a total of 77,313 mouse sequences supplemented with common contaminants from the Max Planck Institute (http://www.coxdocs.org/doku.php?id=maxquant:start_downloads.htm&s[]=contaminants) and the Global Proteome Machine (ftp://ftp.thegpm.org/fasta/cRAP/crap.fasta). The spectral library was then used for spectral matching by MSPLIT-DIA, with spectra passing a 1% FDR threshold subsequently mapped to genes using *ProHits 4.0*.

SAINT analysis by *SAINTexpress* (version 3.6.1[29]) was used to score proximity interactions from MSPLIT-DIA data. Bait runs (three biologic replicates each) were compared against three negative control runs (3xFLAG-only samples). Preys with an FDR ≤5% (Bayesian estimation on the basis of distribution of the averaged SAINT scores across biologic replicates) were considered high-confidence proximity interactions and were presented using dot plots generated using *ProHits-viz*.[30] In *ProHits-viz*, once a prey passes the selected FDR threshold (here 5%) with at least one bait, all its quantitative values across the dataset are retrieved for all baits. Bait-prey proximity interactions falling below the 5% FDR threshold are indicated by the color of the edge. Functional enrichment analysis was performed using *g:Profiler* using the default parameters, but for the exclusion of electronic annotations, and limiting searches

to terms with <1000 genes. AP-MS data have been deposited to the Mass Spectrometry Interactive Virtual Environment (MassIVE) repository (https://massive.ucsd.edu/ProteoSAFe/static/massive.jsp) and assigned the accession number MSV000088163.

Semiquantitative Real-Time RT-PCR

For mRNA isolation, kidney cortex was dissected from mice ($n=3$ per genotype), immediately flash frozen, and stored at −80°C. mRNA was isolated using the PureLink RNA Mini Kit (Invitrogen) and cDNA synthesis was performed on 1-μg RNA with the Superscript II Kit (Invitrogen) using random primers. Semiquantitative real-time RT-PCR reactions were carried out on 1:10 diluted cDNA samples using SsoFast EvaGreen Supermix (Bio-Rad) and the StepOnePlus system (Thermo Fisher). Primer sequences used in this study were designed independently or selected from verified Harvard PrimerBank sets (https://pga.mgh.harvard.edu/primerbank/) and are listed in Supplemental Table 5. Melt curves were examined to verify that there was a single amplicon. Expression differences were calculated using the Δ^{Ct} method. Differences were normalized to the reference genes *Gapdh* and *Hprt*,[17] and fold change was calculated in reference to control samples.

Animals

Doxycycline-inducible, podocyte-specific Nck1/2 dKO (podo-dKO) animals were generated as described previously.[15] Embryonic induction was achieved by providing dox food to dams before day 1 of pregnancy. Nck1 or Nck2 single KO animals (described previously)[13] were backcrossed onto the C57BL/6 background by successive breeding with C57BL/6 male breeders (more than ten rounds; Charles River). All animals were genotyped using previously reported primer pairs and standard methods (Supplemental Table 6).[15,31,32] Because the presence of spontaneous disease was similar in both sexes, both male and female animals were used for analyses. For the nephrotoxic serum (NTS) model of acute injury, males were used in keeping with standard practice for this model.[33] Female littermates were used for LPS and protamine sulfate (PS)/heparin sulfate (HS) experiments in support of the 3Rs of animal research. Animal husbandry was carried out in accordance with Canadian Council on Animal Care guidelines and approved by the University of Guelph Animal Care Committee (AUP#3291).

Evaluation of Proteinuria

Mice were placed into a metabolic cage and allowed to urinate freely. For Coomassie urine gels, urine samples (2 or 5 μl) were diluted in SDS sample buffer, separated by 10% SDS-PAGE, and stained with Coomassie Brilliant Blue R. The urinary albumin-creatinine ratio was determined using the Albuwell M ELISA (Exocell) and Creatinine Companion (Exocell) kits according to the manufacturer's instructions.

Evaluation of Podocyte Loss

Indications of podocyturia were determined by precipitation of proteins from collected urines followed by Western immunoblotting for the podocyte marker Wilms tumor-1 (WT-1), as described previously.[34] Confirmation of podocyte depletion was performed by estimating glomerular podocyte density.[35]

Ultrastructural Analyses

For electron microscopy, kidney cortexes were fixed in 0.1 M sodium cacodylate buffer containing 4% PFA and 2% glutaraldehyde (Electron Microscopy Sciences), postfixed in 1% osmium tetroxide, and dehydrated through graded ethanols. Transmission electron microscopy samples were embedded in Quetol–Spurr resin. Ultrathin sections were cut and stained with uranyl acetate and lead citrate and viewed using a FEI CM100 transmission electron microscope. Effacement was evaluated by quantification of the number of foot processes per micrometer GBM in *ImageJ* from at least three independent glomeruli and at least 100 μm of GBM length. GBM thickness was evaluated by multiple measurements along the basement membrane in the same manner.

LPS Injury Model

Female C57BL/6 WT, Nck1 KO, and Nck2 KO mice between the ages of 3 and 6 months were used for this experiment. Mice were injected intraperitoneally with 200-μg LPS (1 mg/ml in PBS; L2630; Sigma-Aldrich) or an equal volume of PBS. Spot urine samples were collected before injection and at 24 hours after injection, at which time mice were euthanized with CO_2 and samples were collected for ultrastructural analysis.

PS Injury Model

Female (8- to 10-week-old) C57BL/6 WT, Nck1 KO, and Nck2 KO mice were used in this model, which was performed as described previously.[17] Kidneys were removed and immediately processed for analysis after completion of relevant perfusion.

Nephrotoxic Serum Nephrosis

Male (8- to 10-week-old) WT, Nck1 KO, and Nck2 KO mice were injected with 0.04 mg/g of IgG γ2 subclass sheep anti-rat nephrotoxic serum (PTX-001S; Probetex) or an equivalent dose of normal sheep IgG serum as a control (SG0010; Capralogics) *via* intraocular injection. Spot urine samples were collected before and at several time points after injection. Mice were euthanized with CO_2 at the indicated time points and kidneys were removed and immediately processed for analysis.

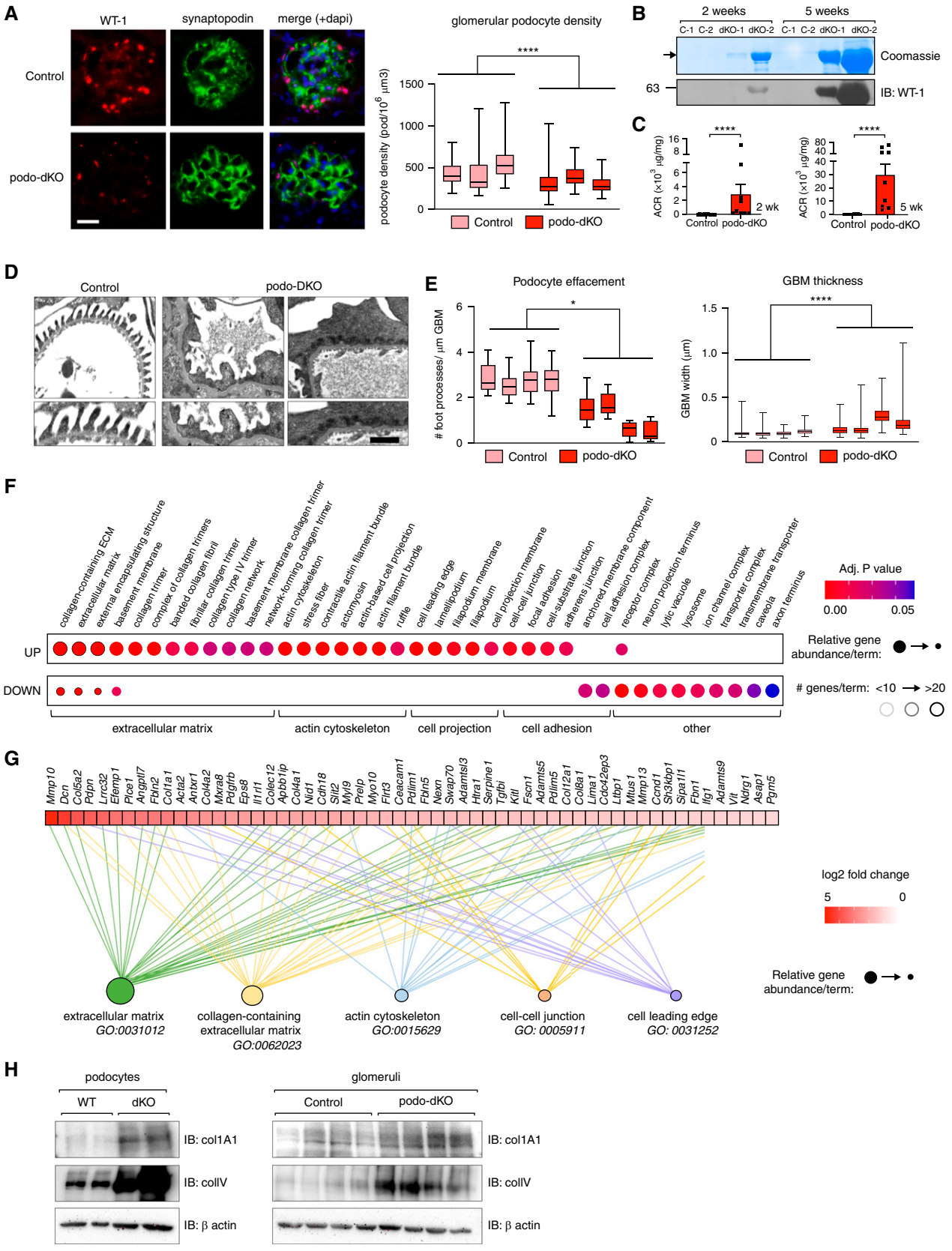

Figure 1. Loss of Nck induces aberrant expression of ECM, cell adhesion, and actin-binding genes within the podocyte. (A) Estimated podocyte density in control and podo-dKO mice at 6 weeks of age determined by analysis of kidney sections immunostained

Figure 1. (*Continued*) for podocyte markers WT-1 and synaptopodin. Box-and-whisker plots represent independent measurements within each animal. ****$P<0.0001$, *by Mann-Whitney two-tailed *t* test. (B) Progressive albuminuria and accompanying podocyte loss in podo-dKO mice compared with controls (C-1, C-2) was shown by Coomassie staining of SDS-PAGE urine gels for albumin and immunoblotting (IB) of urinary precipitates for WT-1. (C) Albuminuria was quantified by albumin-creatinine ratio (ACR) in neonatal (2–3 weeks) and young adult (5–6 weeks) mice. ****$P<0.0001$, by Mann-Whitney two-tailed *t* test. (D–E) Analysis of foot process effacement and GBM thickening in (D) transmission electron micrographs at 5 weeks of age; quantification in (E). Scale bar, 1 μm. Box-and-whisker plots represent independent measurements within each animal. *$P<0.05$ and ****$P<0.0001$, by Mann-Whitney two-tailed *t* test. (F) Dot plot of cellular component GO-enriched terms in gene lists generated from greater than log2 fold change transcriptional changes between WT and dKO podocytes, as identified by microarray. Relative abundance of the number of genes identified for each term in upregulated (UP) versus downregulated (DOWN) (relative to WT) is represented by circle size, total number of terms by border color, and adjusted *P* value by circle color. (G) Genes contributing to the top five cellular component GO-enriched terms were also displayed as heat maps on the basis of fold-change difference in dKO versus WT cells by magnitude. (H) Immunoblotting of collagen 1A1 and type IV collagen in WT and dKO podocytes and control and podo-dKO glomerular lysates. Adj., adjusted.

Statistical Analyses

Data are reported as arithmetic mean±SEM. Data analysis was performed using *GraphPad Prism* version 9.0.2. For all analyses, $P<0.05$ was considered statistically significant. Two groups were compared using unpaired Mann–Whitney *t* test. Three or more groups were analyzed using ANOVA with *post hoc* Tukey HSD test.

RESULTS

Podocyte-Specific KO of Nck1 and Nck2 Causes Podocyte Detachment and GBM Distortion *In Vivo*

We previously generated podo-dKO mice and demonstrated that expression of Nck1 and Nck2 is essential for both podocyte development and maintenance of the glomerular filtration barrier.[13–15] Podo-dKO mice develop nephrotic-range proteinuria, a robust clinical indicator of advanced glomerular disease that is commonly linked with podocyte loss.[36–39] However, the precise molecular mechanisms underlying Nck function in podocytes remain unclear, and it has yet to be established whether proteinuria induced by Nck1/2 KO is accompanied by podocyte depletion. Therefore, we began our investigations by comparing podocyte density in podo-dKO and littermate control mice (Figure 1A). This revealed a reduction in podocyte number in the absence of Nck1/2 by 6 weeks of age. Consistent with this, immunoblotting of urinary sediment with the podocyte marker WT-1 showed evidence of podocytes being shed into the urine as early as 2 weeks after birth (Figure 1B). Notably, this correlated with the degree of proteinuria and became progressively worse with age (Figure 1, B and C), suggesting the observed podocyte hypocellularity could be the result of podocyte detachment from the GBM. Podocyte loss was accompanied by widespread GBM thickening and accumulation of diffuse, electron-dense cytoplasmic aggregates along the basal border of effaced foot processes (Figure 1, D and E). Together, these findings suggest previously unappreciated functions for Nck proteins in GBM ultrastructure and podocyte adhesion.

Loss of Nck1/2 Causes Rewiring of Genes That Govern ECM Deposition, Podocyte Adhesion, and Actin Contractility

To investigate the molecular underpinnings of these pathologic changes in podocytes in the absence of Nck1/2, we generated conditionally immortalized WT and Nck1/Nck2 dKO MPC lines (Supplemental Figure 1, A–D). Because changes in gene expression can inform on changes in cell biology, we performed an Affymetrix GeneChip microarray on these cells. Using a log2 fold change ($P<0.05$) cutoff, we identified the top upregulated (243, 6.5%) and downregulated (158, 3.7%) genes in dKO cells. GO analysis revealed positive enrichment of genes involved in actin binding, actin cellular projection, and cell-cell adherens junctions, in support of our long-held understanding of Nck adaptors as critical regulators of the podocyte cytoskeleton and slit diaphragm (Figure 1F). Moreover, we discovered overrepresentation of basement membrane structural constituents and components of focal adhesions among the top most upregulated genes. Secondary examination by GSEA corroborated these findings (Figure 1G, Supplemental Figure 2B). To determine if these genetic changes translated to differences at the protein level, we performed Western immunoblotting for two of the misregulated ECM components, collagen 1A1 and type IV collagen. In support of our transcriptional findings, both were enriched in lysates from dKO cultured podocytes and podo-dKO glomeruli (Figure 1H). Notably, the enrichment of ECM and focal adhesion terms in our analyses was driven by genes distinct from cytoskeletal terms (Figure 1G), suggesting unexplored Nck-dependent changes in this cellular compartment.

Nck Is Required for Actin and Focal Adhesion Organization and Remodeling during Dynamic Cellular Events

To gain a better understanding of the consequence of these molecular disruptions on podocyte behavior, we performed immunofluorescence staining of F-actin (phalloidin) and focal adhesions (*via* antibody to paxillin) in WT and dKO cells (Figure 2A). dKO cells displayed an increase in focal

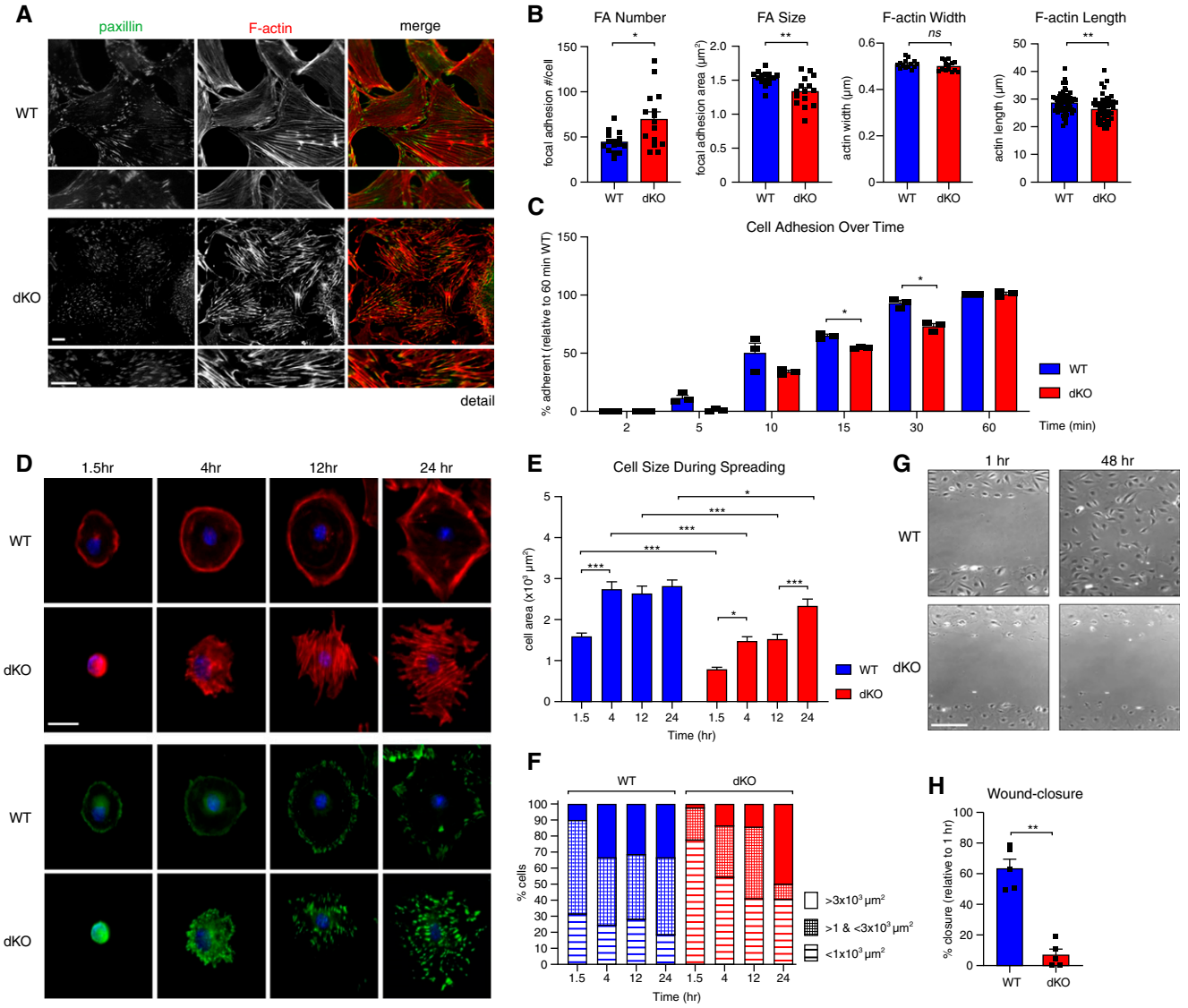

Figure 2. Nck adaptors coordinate actin and focal adhesion turnover during dynamic cellular events. (A) Dual immunofluorescence staining of differentiated WT and Nck1 and Nck2 dKO podocytes for paxillin (focal adhesion marker) and F-actin. Scale bar, 100 μm. (B) Quantification of focal adhesion (FA) number and size and actin stress fiber width and length. *P<0.05, **P<0.01, Mann–Whitney two-tailed t test. (C) Quantification of podocyte adherence to type IV collagen–coated substrate post-trypsinization, over time. **P<0.01, two-way ANOVA and Tukey multiple comparisons test. (D) Immunofluorescence imaging and (E–F) quantification of cell size during spreading on type IV collagen–coated substrate post-trypsinization, over time. *P<0.05, **P<0.01, ***P<0.001, two-way ANOVA and Tukey multiple comparisons test. (G) Representative brightfield images and (H) quantification of differentiated WT and dKO podocytes during *in vitro* wound healing assay. **P<0.01, Mann–Whitney two-tailed t test.

adhesion number and a decrease in focal adhesion size (Figure 2B). This was accompanied by replacement of cortical and dendritic actin structures with disorganized and shortened actin bundles and abnormal cell projections (Figure 2B). Using live-cell imaging, we noted that paxillin-positive adhesions (paxillin-mCherry) were less dynamic (Supplemental Video), a characteristic that parallels findings in Nck-deficient endothelial cells.[40] Altogether, these findings denote disrupted actin and focal adhesion behavior in the absence of Nck.

Central to the dynamic response of podocytes to strain *in vivo* is the dis- and reassembly of their focal adhesions.[41] Therefore, to test whether the static defects observed in dKO podocytes were accompanied by defects in dynamic engagement of their focal adhesions and associated actin cytoskeleton, we performed *in vitro* adhesion, spreading, and migration challenges. In the absence of Nck1/2, podocytes exhibited defective adhesion to type IV collagen (Figure 2C) and delayed spreading thereafter (Figure 2, D–F). Spreading dKO cells displayed enhanced actin bundling and the

accumulation of enlarged, interiorly localized focal adhesions, as compared with the cortical actin, tangential stress fibers, and outward ring of focal adhesions that typifies focal adhesion treadmilling in WT cells (Figure 2D).[42,43] Finally, in wound healing assays, dKO cells were incapable of reorganizing to minimize the opening (Figure 2, G–H). Together, these findings suggest loss of Nck1/2 is accompanied by the upregulation of cell-substrate and actin-associated gene expression, and the accumulation of actin stress fibers and focal adhesions with reduced functionality.

Nck1 and Nck2 Impart Multifaceted Regulation of α Actinin-4/β1-Integrin within the Podocyte

As SH2 and SH3 domain-containing adaptors, Nck proteins bridge a myriad of protein interactions to enact signaling cascades. We used unbiased AP-MS (see *Methods*) to uncover podocyte-specific protein interactomes for each Nck paralog (Supplemental Figure 4, A and B). As expected, we recovered well-documented interactions between Nck1 and/or Nck2 and βPix[8,44] (gene *Arhgef7*); Dok1[45]; the Git,[46,47] Chn, and Pak[48,49] protein families; and the Arp2/3 complex and its regulators N-WASp (gene *Wasl*) and WAVE components,[50,51] including Cyfip1 and Nckap1 (Figure 3A). We also uncovered novel interaction partners, including the SH2 domain–containing protein Shf and actin-binding proteins Plekhh2, palladin (gene *Palld*), and eplin (gene *Lima1*) (Figure 3A). Consistent with the functional defects observed in dKO podocytes, GO analysis of each set of protein interactors supported roles for Nck1 and Nck2 in regulation of actin filament length and organization, and their localization to focal adhesions (Supplemental Figure 4C). To this point, eplin (gene *Lima1*), which was identified as a novel interaction partner of Nck1, was recently classified as a *bona fide* component of the integrin adhesome through its association with the consensus component palladin (gene *Palld*),[44] which we also identified as a novel interactor of Nck2. Interestingly, expression of *Lima1* was identified as highly upregulated in dKO cells (Figure 1G), suggesting multifaceted regulation of focal adhesion components by Nck1/2.

For a more comprehensive view of the intersection of Nck1/2 with podocyte focal adhesions, we next overlaid our transcriptomic and proteomic findings on a current model of the β1-integrin adhesome (Figure 3B, expanded comparison in Supplemental Figure 4, E–F).[52] As has been previously shown, Nck1 and Nck2 each associated with components of the βPix/Git/Pak signaling complex (Supplemental Figure 4D).[8,44] In addition, we now demonstrate their ability to partner with key components of the α actinin-4/β1-integrin signaling module. Interestingly, individual components from the α actinin-4 hub preferentially associated with each Nck paralog. This suggests that, although Nck1 and Nck2 can reside together within this signaling complex, each harbor unique interactions that may contribute to distinct functions. This raises the possibility that both Nck1 and Nck2 may be required to achieve the full repertoire of molecular decisions required to effectively mount dynamic adhesive responses within the podocyte.

Nck dKO Stress Fiber and Focal Adhesion Derangement Is Associated with Perturbation of α Actinin-4, Eplin, and Palladin

α Actinin-4, palladin, and eplin all bind actin and reportedly act together at the interface of the actin cytoskeleton and integrin adhesions.[44] The entangled network of thick actin bundles observed in *ACTN4* mutant podocytes is similar to those observed in our Nck dKO cells,[53] and mutant *ACTN4* likewise contributes to reduced podocyte spreading and migration *in vitro*.[54] Further, the electron-rich densities observed in podo-dKO mice are highly reminiscent of those observed in mice and patients harboring mutant *ACTN4*.[55] These observations prompted further investigation of Nck1 and Nck2 within the α actinin-4/eplin/palladin signaling axis in podocytes.

After confirming the ability of NCK1 and NCK2 to interact with different eplin and palladin isoforms, respectively (Figure 3C, Supplemental Figures 4G and 5A), we analyzed the effect of Nck1/2 depletion on eplin, palladin, and α actinin-4 protein expression and localization. Previously, we observed modest increases in palladin (0.40-fold increase) and α actinin-4 (0.6-fold increase), accompanied by a more significant increase in eplin gene expression (1.37-fold increase) in dKO cells by microarray. Protein levels of each were more markedly increased in dKO cells, an effect that could be partially reverted by re-expression of FLAG-NCK1 or FLAG-NCK2 (Figure 3, D and E). This was accompanied by accrual of α actinin-4 at sites of disordered focal adhesions and superbundled stress fibers in dKO cells (Figure 3F), a finding confirmed using an actin sedimentation assay (Figure 3G). These findings suggest that depletion of Nck1/2 triggers the accumulation of α actinin-4–containing actin bundles and focal adhesions within podocytes, and that contributions to this accumulation may be by both transcriptional and nontranscriptional means.

Nck Controls α Actinin-4 Stabilization at Stress Fibers and Focal Adhesions *via* Cooperative Modulation of Eplin and Palladin

Given that aberrant nucleation of functionally compromised α actinin-4, eplin, and palladin- containing focal adhesions appears central to the dysfunction of Nck-deficient podocytes, we next questioned whether interrupting the accumulation of these complexes could improve features in dKO cells. To test this theory, we generated a series of CRISPR-Cas9 KO cell lines in the background of dKO cells. Pools of CRISPR-targeted lines, referred to herein as dKO-knockdown lines, were generated by transfection of nontargeting control sgRNA or sgRNA targeting either α actinin-4, eplin, or palladin into Nck dKO podocytes followed by antibiotic selection. Similar to lines in which FLAG-NCK1 or -NCK2 were re-expressed,

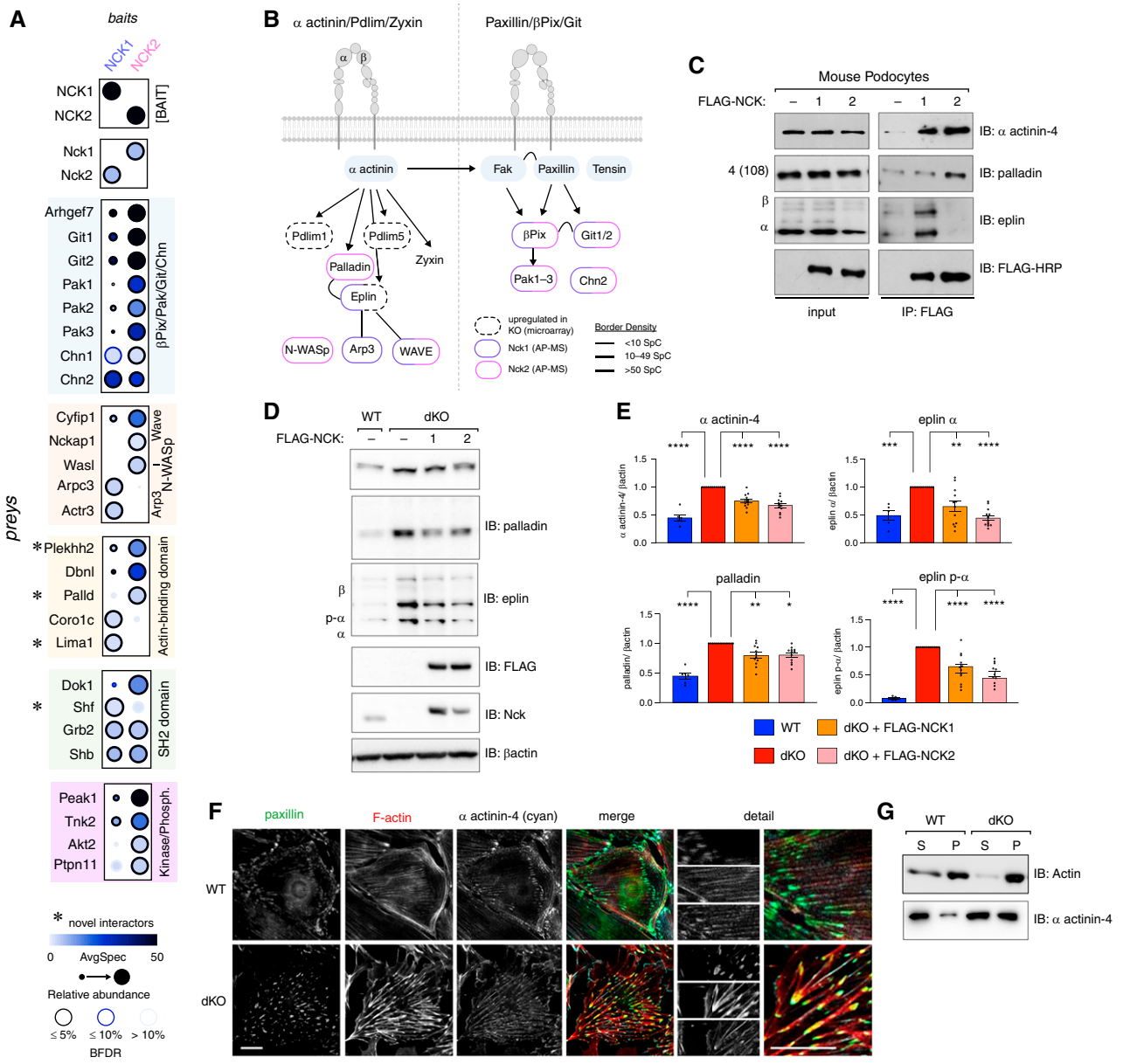

Figure 3. Proteomic identification of Nck1 and Nck2 as novel regulators of actin-binding proteins α actinin-4, eplin, and palladin. (A) Dot plot of identified interactors for NCK1 and NCK2 in podocytes determined by affinity purification mass spectrometry (AP-MS) (gene level, MSPLIT-DIA, BFDR <5%). (B) Overlay of proteomic and transcriptomic findings on integrin adhesion complex modular organization. (C) Coimmunoprecipitation (IP) of NCK1 or NCK2 with eplin or palladin in podocytes. (D) Immunoblotting (IB) and (E) densitometric quantification of α actinin-4, palladin, and eplin in Nck1/2 WT, Nck1 and Nck2 dKO, dKO plus FLAG-NCK1, and dKO plus FLAG-NCK2 podocytes. *P<0.05, **P<0.01, ***P<0.001, ****P<0.0001, two-way ANOVA and Tukey multiple comparisons test. (F) Immunofluorescent imaging of WT and dKO podocytes stained for paxillin, F-actin, and α actinin-4. Scale bar, 100 μm. (G) IB of actin and α actinin-4 in supernatant (S; globular actin) and pellet (P; F-actin) fractions from actin sedimentation samples. BFDR, Bayesian false discovery rate.

deletion of α actinin-4 restored eplin and palladin protein levels (Figure 4, A and B) and improved focal adhesion and F-actin organization (Figure 4, C–F) in dKO cells, suggesting a central role for α actinin-4 accumulation in this phenotype. Knockdown of eplin, but not palladin, led to modest reciprocal normalization of α actinin-4 levels in dKO cells, although stress fibers and focal adhesion organization remained somewhat perturbed (potentially due to partial knockdown, or eplin's actin-related functions that are independent of Nck; Figure 5, A–D). Interestingly, reintroduction of NCK1 or NCK2 in dKO/palladin knockdown cells no longer normalized α actinin-4 or eplin levels (Figure 5, A and B). This

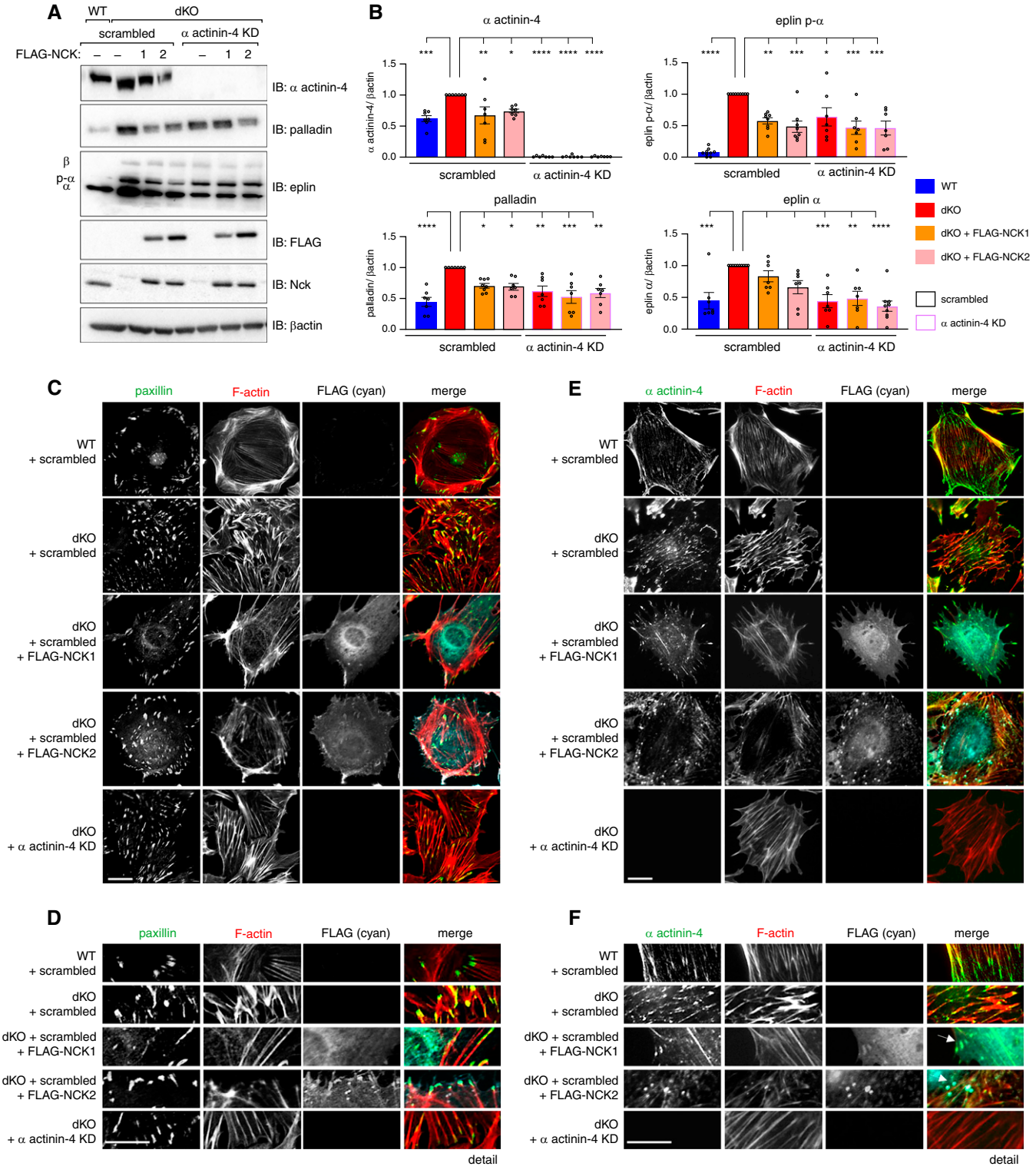

Figure 4. Nck governs α actinin-4–directed actin bundling at stress fibers and focal adhesions. Comparison of protein levels by (A) immunoblot (IB) and (B) densitometric analysis in Nck1/2 dKO cells subjected to scrambled/nontargeting treatment (red bars, black outline) with α actinin-4 knockdown (KD) cells (red bars, purple outline) demonstrates normalization of palladin and eplin protein levels with depletion of α actinin-4 (relative to levels in WT cells [blue bars]). Similar results were achieved in dKO cells rescued with FLAG-NCK1 (orange bars) or FLAG-NCK2 (pink bars). $P<0.05$, $^{**}P<0.01$, $^{***}P<0.001$, $^{****}P<0.0001$, two-way ANOVA and Tukey multiple comparisons test. (C–F) Immunofluorescence of WT (+scrambled) and dKO (+scrambled or α actinin-4 KD) cells with indicated rescues (FLAG-NCK1 or FLAG-NCK2). Arrows demark punctae containing F-actin, Nck, and α actinin-4. Scale bar, 100 μm.

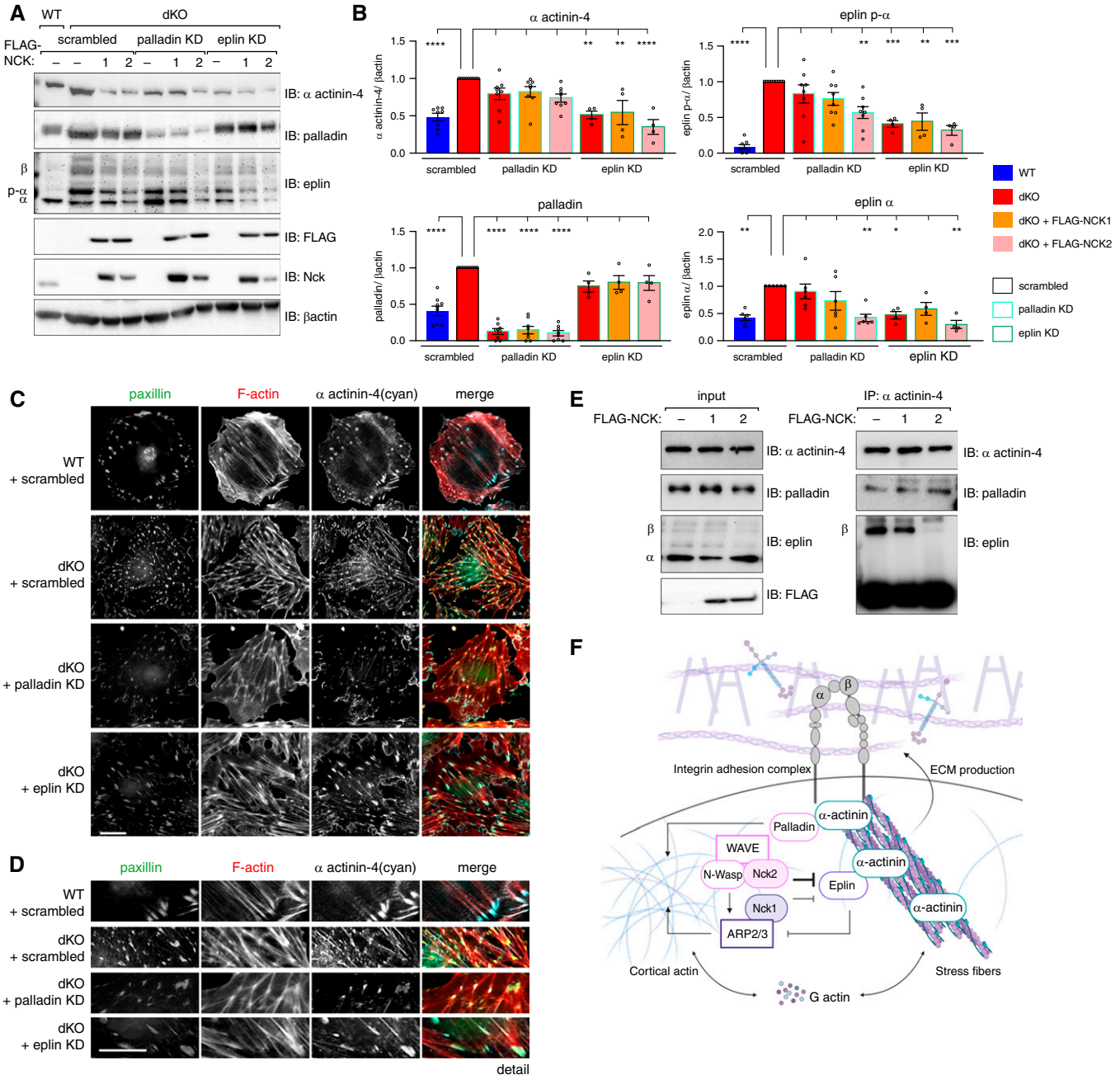

Figure 5. Eplin and palladin differentially modulate α actinin-4. Comparison of protein levels (A) by immunoblot (IB) and (B) densitometric analysis in Nck1/2 dKO cells subjected to scrambled treatment (red bars, black outline) with palladin knockdown (KD) cells (red bars, blue outline) demonstrates normalization of α actinin-4 levels only in the presence of FLAG-NCK2 (pink bar, blue outline). Conversely, comparison of protein levels in dKO plus eplin KD cells (red bars, green outline) with dKO scrambled cells demonstrates modest normalization of α actinin-4 levels, but not those of palladin. This is independent of re-expression of FLAG-NCK1 (orange bar, green outline) or FLAG-NCK2 (pink bar, green outline). *$P<0.05$, **$P<0.01$, ***$P<0.001$, ****$P<0.0001$, two-way ANOVA and Tukey multiple comparisons test. (C–D) Immunofluorescence imaging of WT (+scrambled) and dKO (+scrambled or +palladin KD, or +eplin KD) cells. Scale bar, 100 μm. (E) Co-immunoprecipitation (IP) and IB of α actinin-4 and palladin or eplin in WT cells overexpressing FLAG-NCK1, FLAG-NCK2, or FLAG control. (F) Graphic summary of Nck-mediated regulation of the α actinin-4/β1-integrin module within the podocyte.

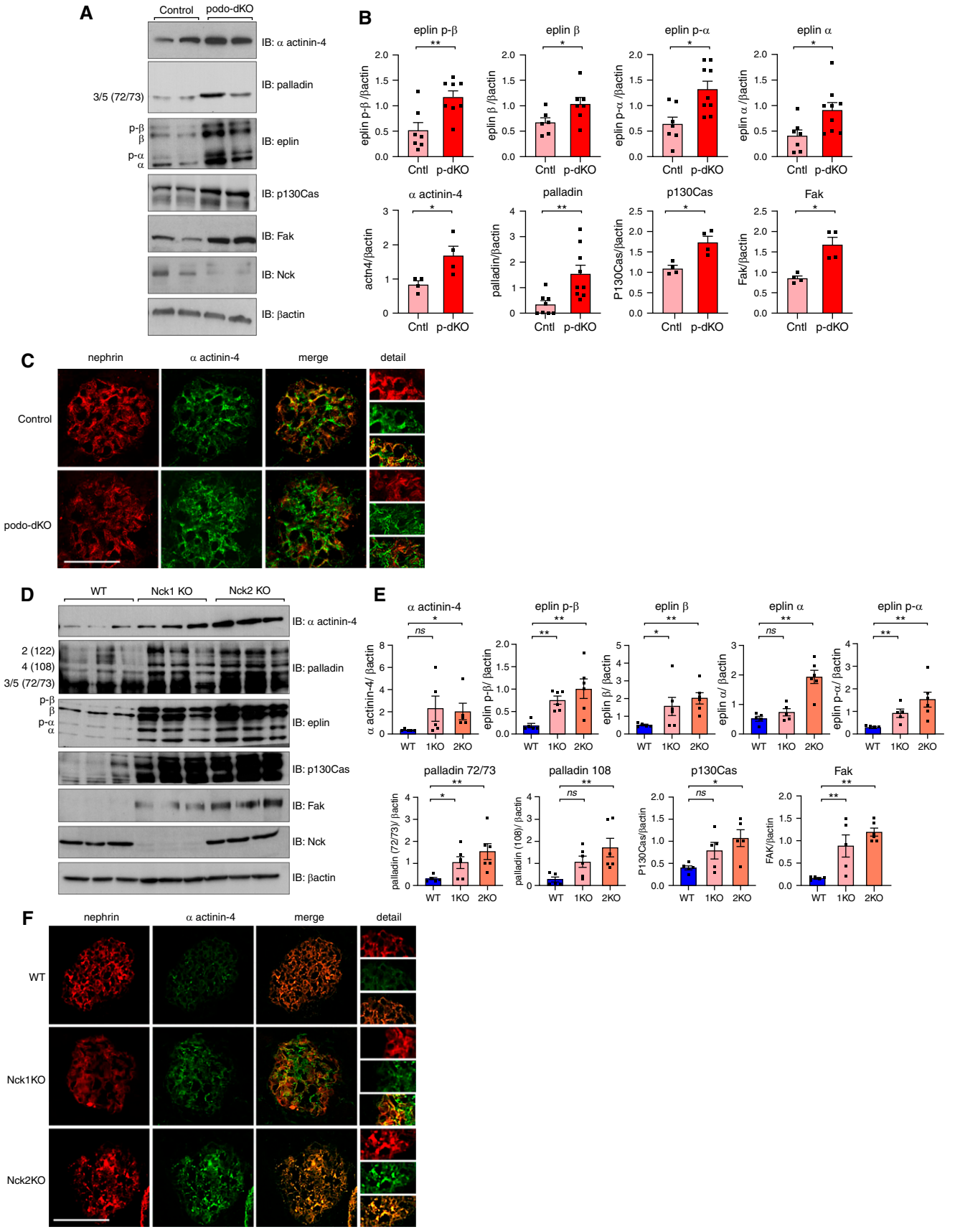
A
Control
podo-dKO
IB: α actinin-4
3/5 (72/73)
IB: palladin
p-β
β
p-α
α
IB: eplin
IB: p130Cas
IB: Fak
IB: Nck
IB: βactin
B
eplin p-β
eplin β
eplin p-α
eplin α
α actinin-4
palladin
p130Cas
Fak
Cntl
p-dKO
C
nephrin
α actinin-4
merge
detail
Control
podo-dKO
D
WT
Nck1 KO
Nck2 KO
IB: α actinin-4
2 (122)
4 (108)
3/5 (72/73)
IB: palladin
IB: eplin
IB: p130Cas
IB: Fak
IB: Nck
IB: βactin
E
α actinin-4
eplin p-β
eplin β
eplin α
eplin p-α
palladin 72/73
palladin 108
p130Cas
Fak
WT
1KO
2KO
F
nephrin
α actinin-4
merge
detail
WT
Nck1KO
Nck2KO

Figure 6.

Figure 6. Depletion of Nck1 and/or Nck2 triggers accrual of α actinin-4 and focal adhesion componentry in mouse glomeruli. (A) Immunoblotting (IB) and (B) densitometric quantification of glomerular lysates from 5-week-old control and podo-dKO mice. *$P<0.05$, **$P<0.01$, Mann–Whitney two-tailed *t* test. (C) Dual immunofluorescence microscopy of kidney sections stained for α actinin-4 and nephrin in control and podo-dKO mice. Scale bar, 100 μm. (D) IB and (E) densitometric quantification of glomerular lysates from 12-month-old WT, Nck1 KO, and Nck2 KO animals. *$P<0.05$, **$P<0.01$, Mann–Whitney two-tailed *t* test. (F) Immunofluorescence microscopy of kidney sections stained for α actinin-4 and nephrin in WT, Nck1 KO, and Nck2 KO mice.

suggests that, although eplin accumulation likely contributes to sustained α actinin-4 accumulation in dKO cells, palladin is conversely required for Nck-mediated normalization of focal adhesions and F-actin in podocytes.

Given that Nck1/2 and α actinin-4 are each capable of binding eplin and palladin, we next asked whether competition for a shared pool of proteins might contribute to their function within the podocyte. Although palladin's interaction with α actinin-4 appears unaffected by the expression of NCK1/2 in WT cells, eplin β's interaction was significantly impaired by overexpression of NCK2, and, to a lesser extent, NCK1 (Figure 5E). This suggests Nck1 and Nck2 may work to modulate actin stabilization at α actinin-4 by the restriction of eplin β's recruitment, although this mechanism requires further investigation.

Taken together, we hypothesize that Nck requires its interaction with palladin to regulate α actinin-4 signaling (Figure 5F). Conversely, Nck limits eplin/α actinin-4 complex formation, thereby preventing haphazard F-actin and focal adhesion accumulation within the cell.

Loss of Nck1 and/or Nck2 *In Vivo* Results in Disrupted α Actinin-4 Signaling and Ultrastructural Abnormalities

Our final objective was to confirm the biochemical findings from our cellular characterizations *in vivo*, beginning with glomeruli of podo-dKO mice. Increased levels of α actinin-4, palladin, and eplin were observed, along with core focal adhesion components p130Cas and FAK, suggesting the accumulation of focal adhesions in the absence of Nck1/2 *in vivo* (Figure 6, A and B). Likewise, discontinuous staining and deposits of α actinin-4 were observed throughout podo-dKO glomeruli, validating our *in vitro* characterizations (Figure 6C). Considering our biochemical analyses suggest cooperative functions for Nck1 and Nck2, we speculated that loss of individual paralogs might also cause disruptions of glomerular integrity over time. Examining Nck1 and Nck2 single KO animals throughout aging, we observed increased levels of eplin and palladin in young adult animals (Supplemental Figure 5, B and C), a phenotype that intensified with age (Figure 6, D and E). Disruption of α actinin-4 levels and organization were observed with KO of Nck1 and/or Nck2, with podo-dKOs displaying the most notable perturbation, followed by Nck2 KO mice (Figure 6, C and F). Notably, although α actinin-4 and focal adhesion components FAK and p130Cas were only modestly altered in young single KO animals (Supplemental Figure 5, B and C), levels were greatly enhanced by 12 months of age (Figure 6, D and E). This suggests eplin and palladin upregulation precedes accumulation of α actinin-4 and focal adhesions *in vivo*. Consistent with our *in vitro* characterizations (Figure 3D), perturbations were generally greater in Nck2 KOs than Nck1 KOs, which collectively exhibited dampened disruptions compared with podo-dKO animals.

We also assessed whether ultrastructural alterations accompany changes in protein expression in single KO animals, as was observed in podo-dKO mice. Although proteinuria was not observed (Figure 7A), segmental GBM thickening was present in Nck1 KO and Nck2 KO mice by 12 months of age (Figure 7, B and C). In addition to enhanced GBM thickening in the absence of Nck2 versus Nck1, Nck2 KO animals displayed modest foot process effacement (Figure 7D), indicating an elevated requirement for Nck2, in line with findings from our cellular work. Seeking to better understand the basis of these GBM alterations, we performed semiquantitative real-time RT-PCR for matrix[56] and adhesion componentry, guided by changes identified within our earlier microarray. This revealed heightened expression of type I and IV collagens, fibronectin, matrix metalloproteases 2 and 13, and αV and β1 integrins, and decreases in expression of laminin α5 and β1, potentially signaling a transition of the podocyte-GBM interface toward a more fibrotic nature in the absence of Nck1 or Nck2 (Figure 7E). Protein-level increases in glomerular collagen 1A1 and type IV collagen were likewise observed, whereas laminin α5, a component of the healthy, mature GBM, decreased (Figure 7, F and G). Increased intensity in staining for both 1A1 and type IV collagens was observed in podocytes (on the basis of costaining with podocin or synaptopodin, respectively, as highlighted in Figure 7G insets), although it should be noted that additional glomerular locales also appeared to show increased levels. Together, these findings highlight singular roles for Nck1 and Nck2 in actin signaling and matrix deposition *in vivo*.

Loss of Nck1 or Nck2 Results in Greater Susceptibility to Podocyte Injury

Cell-matrix interactions play critical roles in podocyte injury and recovery because both require cell process retraction and re-establishment, necessitating focal adhesion dis- and reassembly.[41] Capitalizing on the limited effect of loss of either Nck1 or Nck2 at 2 months of age and lack of proteinuria throughout aging, we next evaluated the requirement of

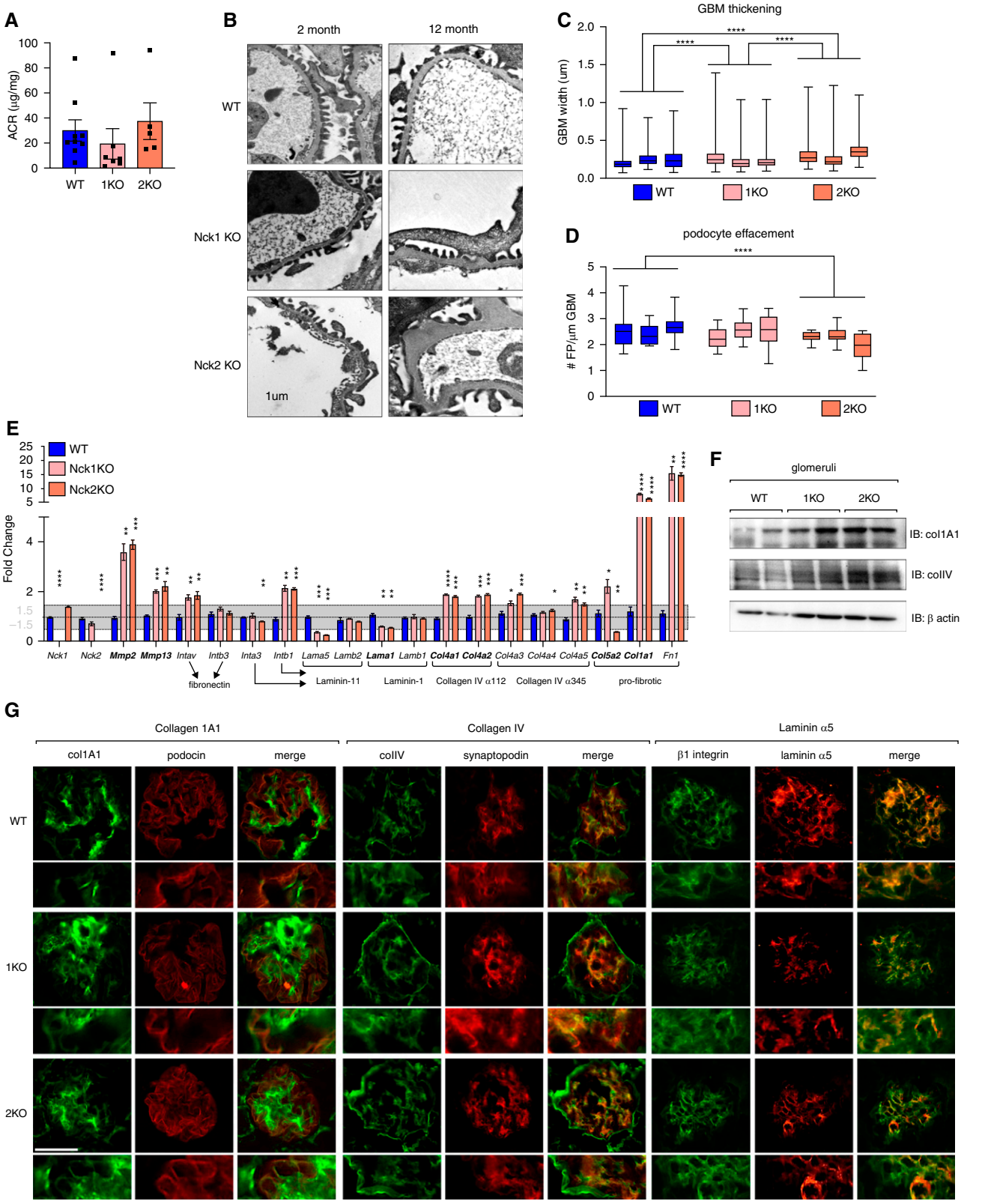

Figure 7. Knockout of Nck1 or Nck2 results in GBM abnormalities during aging, and is accompanied by mild foot process effacement in the absence of Nck2 but not Nck1. (A) Albumin-creatinine ratios (ACR) of urine from 12-month-old WT, Nck1 KO, and Nck2 KO mice demonstrate the lack of proteinuria in all genotypes during aging. (B) Transmission electron micrographs of 2- and 12-month-old mice, accompanied by quantification of (C) podocyte effacement and (D) GBM thickening. Scale bar, 1 μm.

Figure 7. (*Continued*) ****$P<0.0001$, two-way ANOVA and Tukey multiple comparisons test. Box-and-whisker plots represent independent measurements within each animal. (E) Real-time RT-PCR of kidney cortex samples (2-month-old WT, Nck1 KO, and Nck2 KO mice). Genes identified as altered in the preceding microarray are in bold font. Relationships between adhesion genes and the matrix ligands they bind are indicated by arrows. *$P<0.05$, **$P<0.01$, ***$P<0.001$, ****$P<0.0001$, two-way ANOVA and Tukey multiple comparisons test. (F) Immunoblotting (IB) of collagen 1A1 and type IV collagen in WT, Nck1 KO, and Nck2 KO glomerular lysates. (G) Dual immunofluorescence microscopy of kidney sections stained for collagen 1A1, type IV collagen, and laminin α5 from WT, Nck1 KO (1KO), and Nck2 KO (2KO) mice. Scale bar, 100 μm.

each Nck paralog in the podocyte in response to injury using three independent models of podocyte injury in young adult animals. We first used the PS/HS model of reversible foot process effacement to evaluate the ability of young Nck animals to develop and recover from rapid foot process flattening. Both Nck1 KO and Nck2 KO mice displayed enhanced foot process simplification, as compared with WT mice, in response to injury by PS (Figure 8, A and B). Interestingly, although Nck1 KOs recovered as expected after perfusion with HS, effacement persisted in Nck2 KO animals, suggesting a stricter requirement for Nck2 in regulation of the podocyte's actin machinery during recovery. Further, Nck2 KO animals perfused with vehicle alone (HBSS) also demonstrated evidence of increased foot process flattening, which may be explained by an increased susceptibility in these animals during perfusion.

We then monitored the response of single KO animals to LPS-induced nephropathy. At the peak time points of 24–48 hours, Nck2 KO animals showed a marked increase in proteinuria, albuminuria, and effacement as compared with WT animals (Figure 8, C and D). Nck1 KOs showed a more varied response, with animals displaying similar or higher albuminuria than WT counterparts.

Lastly, we performed the low-dose NTS model of nephropathy. Albuminuria was heightened in single KO animals throughout the disease course, with albuminuria being greatest in Nck2 KOs (Figure 8, E and F). Notably, proteinuria was not observed in animals with a single copy of each paralog, excluding the possibility that haploinsufficiency might confer disease predisposition (Supplemental Figure 5D). To determine the contribution of eplin, palladin, and α actinin-4 in disease development, we investigated protein expression in glomerular lysates from WT animals at 24 hours, the peak of disease (Figure 8, G and H). Increased levels of each were apparent, supporting the hypothesis that aberrant activation of adhesive complexes contributes to foot process effacement and filtration barrier disruption during disease, and that loss of Nck1 or Nck2 leaves animals primed for barrier demise.

DISCUSSION

Establishment and maintenance of the glomerular filtration barrier requires coordination between the endothelium, podocytes, and the GBM. Linkage between the GBM and the actin cytoskeleton provides podocytes with physical reinforcement, enabling them to withstand considerable mechanical strain.[57,58] Inversely, maintenance of podocyte tension through coordination of actin and focal adhesions provides the rigidity the GBM requires to maintain its pore size.[59] With disease and accompanying cytoskeletal derangements, injured podocytes develop reduced contractile strength,[10,60] which alters tension within the GBM and permits leakage of molecules into the urine.[59,61] We now demonstrate that Nck1 and Nck2 cooperate to synchronize podocyte ECM deposition and control cell adhesion in a mechanism involving regulation of α actinin-4. α Actinin-4 contributes to podocyte contractility by regulating actin viscoelasticity[62,63] and mutations in its actin-binding domain cause progressive kidney disease–associated stiffening and solidification of the actin network, rendering it more brittle.[62–67] In support of our findings, recent work has demonstrated that α actinin-4's recruitment to integrin adhesion complexes directly contributes to matrix assembly by podocytes.[11] Our results suggest central roles for Nck1 and Nck2 in this mechanism and in regulation of podocyte adhesion by acting as a bridge connecting inputs from integrin/α actinin-4 to the podocyte's actin cytoskeleton.

Our *in vitro* and *in vivo* studies uncovered increased expression and production of cell-substrate adhesion proteins in the absence of Nck1 and/or Nck2, a common consequence of loss of essential focal adhesion constituents.[68,69] The ECM-related genes identified as perturbed in dKO podocytes are well-documented components of the kidney's dual-layered GBM.[56,70] In humans, collagen IV, collagen α121, and laminin-111 predominate within the arising GBM, whereas the mature GBM comprises two distinct laminin-521 layers surrounding a central collagen IV α345 network.[70] Upon adulthood, GBM biosynthetic programs are downregulated.[71] Unbridled collagen deposition and remodeling (by proteases and matrix metalloproteases) often contribute to distortion of the matrix during disease.[72,73] Although these adaptations have been theorized as an attempt to maintain the barrier after damage, they come at the expense of foot process collapse, podocyte detachment, and irreversible fibrosis, as was observed in podo-dKO animals and single KO animals during aging.

Alongside palladin and eplin, our AP-MS screen identified N-WASp, WAVE, and Arp2/3 complex components as Nck interactors within the podocyte. Similar to α actinin-4,[74] Arp2/3 is enriched in the podocyte proteome[75] and is implicated in alignment of cell-matrix adhesions.[76] Notably, polymerization of cortical actin by Arp2/3 and/or formins in the

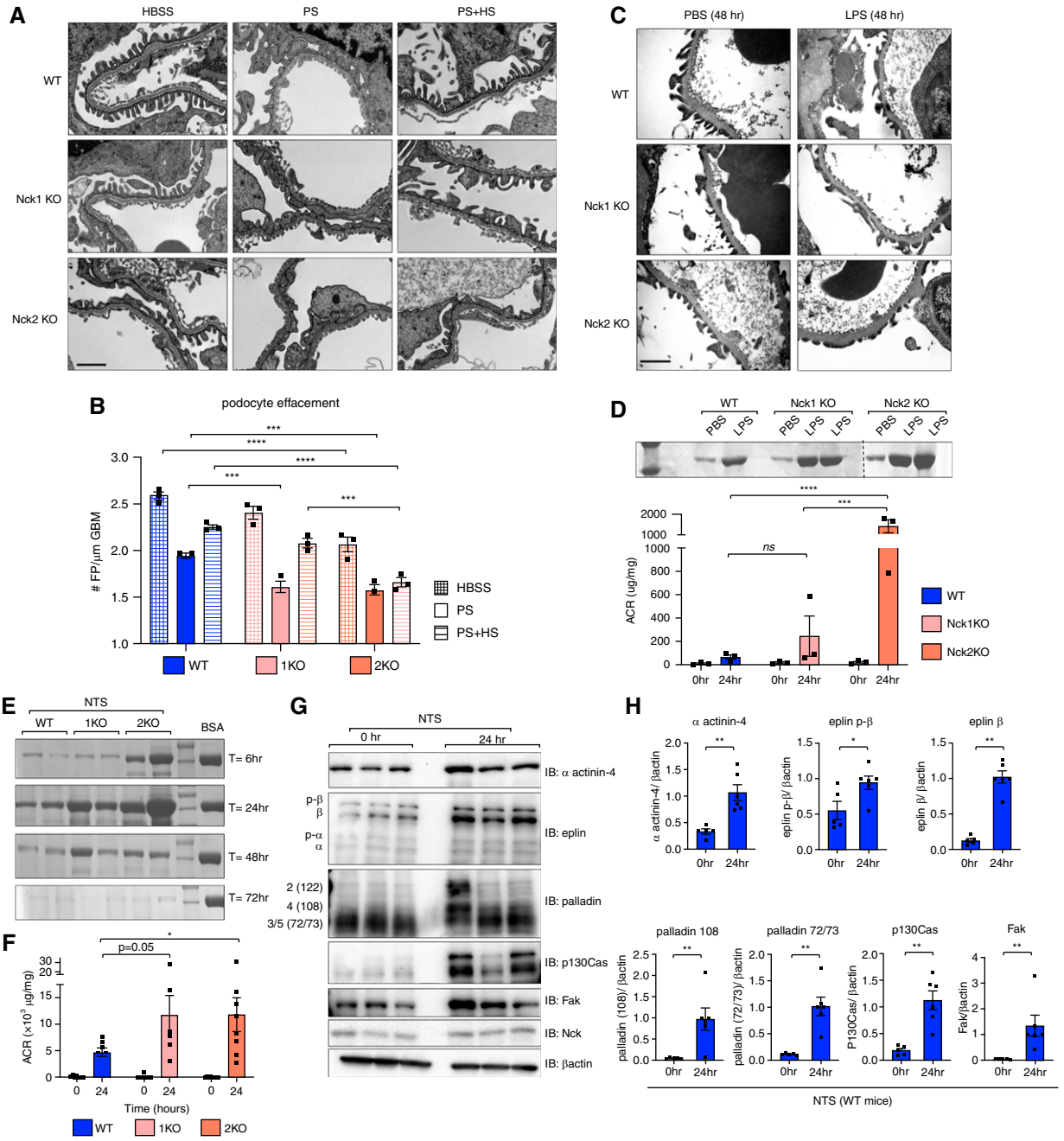

Figure 8. Nck1 and Nck2 KO animals show differential susceptibility to experimental disease models. (A) Transmission electron micrographs showing foot process morphology in WT, Nck1 KO, and Nck2 KO mice after perfusion with PS (injury), PS and HS (recovery), or vehicle alone (HBSS). Scale bar, 1 μm. (B) Quantification of foot process (FP) effacement from (A). ***$P<0.001$, ****$P<0.0001$, two-way ANOVA and Tukey multiple comparisons test. (C) Transmission electron micrographs of mice injected with LPS or vehicle alone (PBS) at the peak injury time point of 48-hours post-injection. (D) A Coomassie urine gel and urinary albumin-creatinine ratio (ACR) demonstrate heightened proteinuria in Nck2 KO mice after LPS-induced disease. ***P<0.001, ****P<0.0001, two-way ANOVA and Tukey multiple comparisons test. (E) Coomassie urine gel displaying albuminuria over the injury (6–24 hours) and recovery periods (48–72 hours) of NTS-induced disease (BSA serves as a positive control). (F) Urinary ACRs at the peak time point of 24 hours after NTS quantify differences between genotypes. *$P<0.05$, two-way ANOVA and Tukey multiple comparisons test. (G) Immunoblotting (IB) and (H) densitometric quantification of glomerular lysates from WT mice pre- and post-NTS injection. *$P<0.05$, **$P<0.01$, Mann–Whitney two-tailed t test. 1KO, Nck1 KO; 2KO, Nck2 KO.

membrane vicinity precedes formation of focal adhesions. The physical appearance and functional disruptions in dKO cells are strikingly similar to those described in a recent report characterizing the podocyte-specific function of Arp3.[75] Paralleling our observations in Nck dKO cells, Arp3 deficiency results in loss of dendritic actin networks in the cell cortex, increased actomyosin contractility, and changes in focal adhesion morphology, leading to podocyte detachment and perinatal effacement and proteinuria.[75] Whereas palladin is reported to act in a compensatory manner in actin branching in the absence of Arp2/3,[77] eplin binds and inhibits Arp2/3's actin-branching capability.[78] Our results suggest eplin's ability to bind α actinin-4 is directly affected by Nck and we question whether a similar relationship with Arp2/3 might exist, given our findings of enhanced eplin levels and reduced cytoskeletal plasticity in dKO cells. Further, we question whether palladin upregulation may be a mechanism to compensate for reduced Arp2/3 activity in the absence of Nck.

Interestingly, recent work has demonstrated that integrin complexes communicate with the slit diaphragm protein nephrin to coordinate integrin activation and nephrin tyrosine phosphorylation.[79,80] Given the well-established role of Nck in nephrin signaling,[13,81,82] and the requirement for nephrin signaling in maintenance of foot process structure and barrier function,[17] it is tempting to speculate on the potential for Nck to act as a bridge between the slit diaphragm laterally and focal adhesions basally localized along the GBM, a theory deserving of further study. However, owing to Nck's importance within multiple key signaling nodes in podocytes, it is difficult to distinguish which actions of Nck might be most critical to podocyte function. Nevertheless, our *in vitro* podocyte findings (in a context where nephrin is not expressed) provide evidence that the involvement of Nck in α actinin-4–mediated focal adhesion dynamics occurs independently of nephrin. Overall, these findings expand on Nck's role in the podocyte beyond the slit diaphragm and provide a more comprehensive molecular picture of Nck1 and Nck2's functions.

Finally, our results point to complementary rather than compensatory roles for Nck1 and Nck2 in regulation of actin and focal adhesions within podocytes. Loss of Nck2 resulted in greater damage and reduced recovery compared with KO of Nck1 *in vivo*. Further, Nck2 rescue in dKO cells led to superior normalization of palladin, eplin, and α actinin-4 levels; enhanced redirection of α actinin-4 into actin-associated puncta; and reduction of α actinin-4/eplin complex formation. Future studies will continue to investigate these mechanisms to better elucidate these newly identified functions for Nck adaptors and their essentiality within podocytes.

DISCLOSURES

A.-C. Gingras reports having consultancy agreements with and receiving honoraria from 908Devices (instrumentation for mass spectrometry); receiving honoraria from public organizations, including the American Society for Biochemistry and Molecular Biology, the European Research Council, and granting agencies (compensation for grant reviews); serving in an advisory or leadership role as chair of the Canadian Institutes of Health Research (CIHR) Institute of Genetics Advisory Board, the lead for the functional genomics pillar of CoVaRR-Net, deputy editor for *Molecular and Cellular Proteomics*, advisor for the journals *Molecular Cell* and *Molecular Systems Biology*, and chair of the scientific advisory board (SAB) of the National Research Council of Canada Human Health Therapeutics; receiving research funding from Providence Therapeutics (contractual work for the vaccine company); and serving on the SABs of several international large grants (Horizon 2020, National Institutes of Health P41). N. Phippen reports having ownership interest in Century Therapeutics, and being employed by Century Therapeutics and the University of Guelph. M. Platt reports being employed by Creative Destruction Lab. All remaining authors have nothing to disclose.

FUNDING

This work was supported by Kidney Foundation of Canada biomedical research grants KFOC150012, KFOC170010, and KFOC190002 (all to N. Jones). M. Krendel was supported by National Institute of Diabetes and Digestive and Kidney Diseases grant R01DK083345.

ACKNOWLEDGMENTS

We thank Dr. Louise Larose for generously providing the Nck antibody.[83] We also express gratitude to the staff at the University of Guelph Central Animal Facility, without which this research would not be possible.

We acknowledge that the correlation between Nck depletion and α actinin-4 accumulation was initially discovered while C.E. Martin was receiving training at the laboratory of Dr. Chris Kennedy at the University of Ottawa as a visiting research student. This opportunity was essential to the trajectory of this project. N. Jones holds a Canada Research Chair (CRC) in Eukaryotic Cellular Signaling and was the recipient of a CIHR/KRESCENT New Investigator Award. A.-C. Gingras holds a CRC in Functional Proteomics. N. Bisson holds a CRC in Cancer Proteomics. C.E. Martin was supported by a Natural Sciences and Engineering Research Council of Canada Graduate Student Doctoral Award, a Canadian Institutes of Health Research Fellowship, and KRESCENT fellowship awards. A. Keyvani Chahi was supported by an Ontario Graduate Scholarship. Images were generated with BioRender.com (agreement number SY23P EZIF5).

AUTHOR CONTRIBUTIONS

S.L. Banerjee, A. Keyvani Chahi, P. Lu, C.E. Martin, L.A. New, N.J. Phippen, M.J. Platt, J.A. Simpson, M. Tilak, and C.R. Williamson were responsible for investigation; N. Bisson, A.-C. Gingras, N. Jones, M. Krendel, and J.A. Simpson were responsible for resources; A.-C. Gingras was responsible for software; A.-C. Gingras and N. Jones provided supervision; A.-C. Gingras, N. Jones, A. Keyvani Chahi, M. Krendel, C.E. Martin, and L.A. New reviewed and edited the manuscript; A.-C. Gingras, N. Jones, A. Keyvani Chahi, C.E. Martin, and N.J. Phippen were responsible for formal analyses; A.-C. Gingras, N. Jones, and M. Krendel were responsible for funding acquisition; N. Jones was responsible for methodology; N. Jones, A. Keyvani Chahi, and C.E. Martin conceptualized the study; N. Jones and C.E. Martin wrote the original draft and were responsible for validation; A. Keyvani Chahi, C.E. Martin, and M. Tilak

were responsible for data curation; and A. Keyvani Chahi, M. Krendel, P. Lu, C.E. Martin, N.J. Phippen, M. Tilak, and C.R. Williamson were responsible for visualization.

DATA SHARING STATEMENT

Original data reported in this paper have been deposited to MassIVE (accession MSV000088163) and GEO (accession GSE184235).

SUPPLEMENTAL MATERIAL

This article contains the following supplemental material online at http://jasn.asnjournals.org/lookup/suppl/doi:10.1681/ASN.2021101343/-/DCSupplemental.

Supplemental Video 1. Focal adhesions are less dynamic in Nck1/Nck2 double knockout podocytes.

Supplemental Table 1. Antibody information for immunoprecipitation experiments.

Supplemental Table 2. Antibody information for immunoblotting experiments.

Supplemental Table 3. Antibody information for immunofluorescent experiments.

Supplemental Table 4. Sequences used for CRISPR-Cas9 gene editing and TIDE analysis.

Supplemental Table 5. Primers used for semi-quantitative real-time reverse transcriptase polymerase chain reaction.

Supplemental Table 6. Primers used for genotyping.

Supplemental Figure 1. Generation of wild-type and Nck1 and Nck2 double knockout mouse podocyte cell lines.

Supplemental Figure 2. Gene expression analysis of wild-type and Nck1 and Nck2 double knockout podocytes.

Supplemental Figure 3. Normalized enrichment scores from gene set enrichment analysis of microarray data.

Supplemental Figure 4. Multi-faceted contributions of Nck1 and Nck2 to α actinin-4 and β1 integrin-related cell adhesion.

Supplemental Figure 5. Loss of Nck1 or Nck2 (but not Nck1/2 haploinsufficiency) results in biochemical abnormalities and susceptibility to disease.

REFERENCES

1. Martin CE, Jones N: Nephrin signaling in the podocyte: An updated view of signal regulation at the slit diaphragm and beyond. *Front Endocrinol (Lausanne)* 9: 302, 2018
2. Korhonen M, Ylänne J, Laitinen L, Virtanen I: The alpha 1-alpha 6 subunits of integrins are characteristically expressed in distinct segments of developing and adult human nephron. *J Cell Biol* 111: 1245–1254, 1990
3. Baraldi A, Furci L, Zambruno G, Rubbiani E, Annessi G, Lusvarghi E: Very late activation-3 integrin is the dominant beta 1-integrin on the glomerular capillary wall: An immunofluorescence study in nephrotic syndrome. *Nephron* 62: 382–388, 1992
4. Eftekhari A, Vahed SZ, Kavetskyy T, Rameshrad M, Jafari S, Chodari L, et al.: Cell junction proteins: Crossing the glomerular filtration barrier in diabetic nephropathy. *Int J Biol Macromol* 148: 475–482, 2020
5. Butt L, Unnersjö-Jess D, Höhne M, Edwards A, Binz-Lotter J, Reilly D, et al.: A molecular mechanism explaining albuminuria in kidney disease. *Nat Metab* 2: 461–474, 2020
6. Schell C, Rogg M, Suhm M, Helmstädter M, Sellung D, Yasuda-Yamahara M, et al.: The FERM protein EPB41L5 regulates actomyosin contractility and focal adhesion formation to maintain the kidney filtration barrier. *Proc Natl Acad Sci U S A* 114: E4621–E4630, 2017
7. Hobeika L, Barati MT, Caster DJ, McLeish KR, Merchant ML: Characterization of glomerular extracellular matrix by proteomic analysis of laser-captured microdissected glomeruli. *Kidney Int* 91: 501–511, 2017
8. Horton ER, Humphries JD, James J, Jones MC, Askari JA, Humphries MJ: The integrin adhesome network at a glance. *J Cell Sci* 129: 4159–4163, 2016
9. Feng D, DuMontier C, Pollak MR: The role of alpha-actinin-4 in human kidney disease. *Cell Biosci* 5: 44, 2015
10. Feng D, Notbohm J, Benjamin A, He S, Wang M, Ang L-H, et al.: Disease-causing mutation in α-actinin-4 promotes podocyte detachment through maladaptation to periodic stretch. *Proc Natl Acad Sci U S A* 115: 1517–1522, 2018
11. Maier JI, Rogg M, Helmstädter M, Sammarco A, Schilling O, Sabass B, et al.: EPB41L5 controls podocyte extracellular matrix assembly by adhesome-dependent force transmission. *Cell Rep* 34: 108883, 2021
12. Blasutig IM, New LA, Thanabalasuriar A, Dayarathna TK, Goudreault M, Quaggin SE, et al.: Phosphorylated YDXV motifs and Nck SH2/SH3 adaptors act cooperatively to induce actin reorganization. *Mol Cell Biol* 28: 2035–2046, 2008
13. Jones N, Blasutig IM, Eremina V, Ruston JM, Bladt F, Li H, et al.: Nck adaptor proteins link nephrin to the actin cytoskeleton of kidney podocytes. *Nature* 440: 818–823, 2006
14. Verma R, Kovari I, Soofi A, Nihalani D, Patrie K, Holzman LB: Nephrin ectodomain engagement results in Src kinase activation, nephrin phosphorylation, Nck recruitment, and actin polymerization. *J Clin Invest* 116: 1346–1359, 2006
15. Jones N, New LA, Fortino MA, Eremina V, Ruston J, Blasutig IM, et al.: Nck proteins maintain the adult glomerular filtration barrier. *J Am Soc Nephrol* 20: 1533–1543, 2009
16. Shankland SJ, Pippin JW, Reiser J, Mundel P: Podocytes in culture: Past, present, and future. *Kidney Int* 72: 26–36, 2007
17. New LA, Martin CE, Scott RP, Platt MJ, Keyvani Chahi A, Stringer CD, et al.: Nephrin tyrosine phosphorylation is required to stabilize and restore podocyte foot process architecture. *J Am Soc Nephrol* 27: 2422–2435, 2016
18. Bi J, Pellenz CD, Krendel M: Visualization of cytoskeletal dynamics in podocytes using adenoviral vectors. *Cytoskeleton (Hoboken)* 71: 145–156, 2014
19. Doudna JA, Charpentier E: Genome editing. The new frontier of genome engineering with CRISPR-Cas9. *Science* 346: 1258096, 2014
20. Brinkman EK, van Steensel B: Rapid quantitative evaluation of CRISPR genome editing by TIDE and TIDER. *Methods Mol Biol* 1961: 29–44, 2019
21. Jacquet K, Banerjee SL, Chartier FJM, Elowe S, Bisson N: Proteomic analysis of NCK1/2 adaptors uncovers paralog-specific interactions that reveal a new role for NCK2 in cell abscission during cytokinesis. *Mol Cell Proteomics* 17: 1979–1990, 2018
22. Beigbeder A, Vélot L, James DA, Bisson N: Sample preparation for mass spectrometry analysis of protein-protein interactions in cancer cell lines and tissues. *Methods Mol Biol* 1458: 339–347, 2016
23. Rappsilber J, Mann M, Ishihama Y: Protocol for micro-purification, enrichment, pre-fractionation and storage of peptides for proteomics using StageTips. *Nat Protoc* 2: 1896–1906, 2007
24. Hesketh GG, Papazotos F, Pawling J, Rajendran D, Knight JDR, Martinez S, et al.: The GATOR-Rag GTPase pathway inhibits mTORC1 activation by lysosome-derived amino acids. *Science* 370: 351–356, 2020
25. Wang J, Tucholska M, Knight JDR, Lambert J-P, Tate S, Larsen B, et al.: MSPLIT-DIA: Sensitive peptide identification for data-independent acquisition. *Nat Methods* 12: 1106–1108, 2015
26. Liu G, Knight JDR, Zhang JP, Tsou C-C, Wang J, Lambert J-P, et al.: Data independent acquisition analysis in ProHits 4.0. *J Proteomics* 149: 64–68, 2016

27. Kim S, Mischerikow N, Bandeira N, Navarro JD, Wich L, Mohammed S, et al.: The generating function of CID, ETD, and CID/ETD pairs of tandem mass spectra: Applications to database search. *Mol Cell Proteomics* 9: 2840–2852, 2010
28. Elias JE, Gygi SP: Target-decoy search strategy for increased confidence in large-scale protein identifications by mass spectrometry. *Nat Methods* 4: 207–214, 2007
29. Teo G, Liu G, Zhang J, Nesvizhskii AI, Gingras A-C, Choi H: SAINTexpress: Improvements and additional features in Significance Analysis of INTeractome software. *J Proteomics* 100: 37–43, 2014
30. Knight JDR, Choi H, Gupta GD, Pelletier L, Raught B, Nesvizhskii AI, et al.: ProHits-viz: A suite of web tools for visualizing interaction proteomics data. *Nat Methods* 14: 645–646, 2017
31. Fawcett JP, Georgiou J, Ruston J, Bladt F, Sherman A, Warner N, et al.: Nck adaptor proteins control the organization of neuronal circuits important for walking. *Proc Natl Acad Sci U S A* 104: 20973–20978, 2007
32. Bladt F, Aippersbach E, Gelkop S, Strasser GA, Nash P, Tafuri A, et al.: The murine Nck SH2/SH3 adaptors are important for the development of mesoderm-derived embryonic structures and for regulating the cellular actin network. *Mol Cell Biol* 23: 4586–4597, 2003
33. Pippin JW, Brinkkoetter PT, Cormack-Aboud FC, Durvasula RV, Hauser PV, Kowalewska J, et al.: Inducible rodent models of acquired podocyte diseases. *Am J Physiol Renal Physiol* 296: F213–F229, 2009
34. Robins R, Baldwin C, Aoudjit L, Côté J-F, Gupta IR, Takano T: Rac1 activation in podocytes induces the spectrum of nephrotic syndrome. *Kidney Int* 92: 349–364, 2017
35. Venkatareddy M, Wang S, Yang Y, Patel S, Wickman L, Nishizono R, et al.: Estimating podocyte number and density using a single histologic section. *J Am Soc Nephrol* 25: 1118–1129, 2014
36. Palmer BF: Proteinuria as a therapeutic target in patients with chronic kidney disease. *Am J Nephrol* 27: 287–293, 2007
37. Vogelmann SU, Nelson WJ, Myers BD, Lemley KV: Urinary excretion of viable podocytes in health and renal disease. *Am J Physiol Renal Physiol* 285: F40–F48, 2003
38. Petermann AT, Krofft R, Blonski M, Hiromura K, Vaughn M, Pichler R, et al.: Podocytes that detach in experimental membranous nephropathy are viable. *Kidney Int* 64: 1222–1231, 2003
39. Petermann AT, Pippin J, Krofft R, Blonski M, Griffin S, Durvasula R, et al.: Viable podocytes detach in experimental diabetic nephropathy: Potential mechanism underlying glomerulosclerosis. *Nephron, Exp Nephrol* 98: e114–e123, 2004
40. Chaki SP, Barhoumi R, Berginski ME, Sreenivasappa H, Trache A, Gomez SM, et al.: Nck enables directional cell migration through the coordination of polarized membrane protrusion with adhesion dynamics. *J Cell Sci* 126: 1637–1649, 2013
41. Ma H, Togawa A, Soda K, Zhang J, Lee S, Ma M, et al.: Inhibition of podocyte FAK protects against proteinuria and foot process effacement. *J Am Soc Nephrol* 21: 1145–1156, 2010
42. Livne A, Geiger B: The inner workings of stress fibers - from contractile machinery to focal adhesions and back. *J Cell Sci* 129: 1293–1304, 2016
43. Parsons JT, Horwitz AR, Schwartz MA: Cell adhesion: Integrating cytoskeletal dynamics and cellular tension. *Nat Rev Mol Cell Biol* 11: 633–643, 2010
44. Chastney MR, Lawless C, Humphries JD, Warwood S, Jones MC, Knight D, et al.: Topological features of integrin adhesion complexes revealed by multiplexed proximity biotinylation. *J Cell Biol* 219: e202003038, 2020
45. Lock P, Casagranda F, Dunn AR: Independent SH2-binding sites mediate interaction of Dok-related protein with RasGTPase-activating protein and Nck. *J Biol Chem* 274: 22775–22784, 1999
46. Brown MC, Cary LA, Jamieson JS, Cooper JA, Turner CE: Src and FAK kinases cooperate to phosphorylate paxillin kinase linker, stimulate its focal adhesion localization, and regulate cell spreading and protrusiveness. *Mol Biol Cell* 16: 4316–4328, 2005
47. Frese S, Schubert W-D, Findeis AC, Marquardt T, Roske YS, Stradal TEB, et al.: The phosphotyrosine peptide binding specificity of Nck1 and Nck2 Src homology 2 domains. *J Biol Chem* 281: 18236–18245, 2006
48. Bokoch GM, Wang Y, Bohl BP, Sells MA, Quilliam LA, Knaus UG: Interaction of the Nck adapter protein with p21-activated kinase (PAK1). *J Biol Chem* 271: 25746–25749, 1996
49. Galisteo ML, Chernoff J, Su YC, Skolnik EY, Schlessinger J: The adaptor protein Nck links receptor tyrosine kinases with the serine-threonine kinase Pak1. *J Biol Chem* 271: 20997–21000, 1996
50. Li W, Fan J, Woodley DT: Nck/Dock: An adapter between cell surface receptors and the actin cytoskeleton. *Oncogene* 20: 6403–6417, 2001
51. Chaki SP, Rivera GM: Integration of signaling and cytoskeletal remodeling by Nck in directional cell migration. *Bioarchitecture* 3: 57–63, 2013
52. Humphries JD, Chastney MR, Askari JA, Humphries MJ: Signal transduction via integrin adhesion complexes. *Curr Opin Cell Biol* 56: 14–21, 2019
53. Weins A, Schlöndorff JS, Nakamura F, Denker BM, Hartwig JH, Stossel TP, et al.: Disease-associated mutant alpha-actinin-4 reveals a mechanism for regulating its F-actin-binding affinity. *Proc Natl Acad Sci U S A* 104: 16080–16085, 2007
54. Michaud J-LR, Chaisson KM, Parks RJ, Kennedy CRJ: FSGS-associated alpha-actinin-4 (K256E) impairs cytoskeletal dynamics in podocytes. *Kidney Int* 70: 1054–1061, 2006
55. Henderson JM, Alexander MP, Pollak MR: Patients with ACTN4 mutations demonstrate distinctive features of glomerular injury. *J Am Soc Nephrol* 20: 961–968, 2009
56. Lennon R, Byron A, Humphries JD, Randles MJ, Carisey A, Murphy S, et al.: Global analysis reveals the complexity of the human glomerular extracellular matrix. *J Am Soc Nephrol* 25: 939–951, 2014
57. Endlich K, Kliewe F, Endlich N: Stressed podocytes-mechanical forces, sensors, signaling and response. *Pflugers Arch* 469: 937–949, 2017
58. Feng D, DuMontier C, Pollak MR: Mechanical challenges and cytoskeletal impairments in focal segmental glomerulosclerosis. *Am J Physiol Renal Physiol* 314: F921–F925, 2018
59. Fissell WH, Miner JH: What is the glomerular ultrafiltration barrier? *J Am Soc Nephrol* 29: 2262–2264, 2018
60. Haley KE, Kronenberg NM, Liehm P, Elshani M, Bell C, Harrison DJ, et al.: Podocyte injury elicits loss and recovery of cellular forces. *Sci Adv* 4: eaap8030, 2018
61. Lawrence MG, Altenburg MK, Sanford R, Willett JD, Bleasdale B, Ballou B, et al.: Permeation of macromolecules into the renal glomerular basement membrane and capture by the tubules. *Proc Natl Acad Sci U S A* 114: 2958–2963, 2017
62. Yao NY, Becker DJ, Broedersz CP, Depken M, Mackintosh FC, Pollak MR, et al.: Nonlinear viscoelasticity of actin transiently cross-linked with mutant α-actinin-4. *J Mol Biol* 411: 1062–1071, 2011
63. Ward SMV, Weins A, Pollak MR, Weitz DA: Dynamic viscoelasticity of actin cross-linked with wild-type and disease-causing mutant alpha-actinin-4. *Biophys J* 95: 4915–4923, 2008
64. Kaplan JM, Kim SH, North KN, Rennke H, Correia LA, Tong HQ, et al.: Mutations in ACTN4, encoding alpha-actinin-4, cause familial focal segmental glomerulosclerosis. *Nat Genet* 24: 251–256, 2000
65. Weins A, Kenlan P, Herbert S, Le TC, Villegas I, Kaplan BS, et al.: Mutational and biological analysis of alpha-actinin-4 in focal segmental glomerulosclerosis. *J Am Soc Nephrol* 16: 3694–3701, 2005
66. Choi HJ, Lee BH, Cho HY, Moon KC, Ha I-S, Nagata M, et al.: Familial focal segmental glomerulosclerosis associated with an ACTN4 mutation and paternal germline mosaicism. *Am J Kidney Dis* 51: 834–838, 2008
67. Feng D, Steinke JM, Krishnan R, Birrane G, Pollak MR: Functional validation of an alpha-actinin-4 mutation as a potential cause of an aggressive presentation of adolescent focal segmental glomerulosclerosis: Implications for genetic testing. *PLoS One* 11: e0167467, 2016

68. Quach NL, Biressi S, Reichardt LF, Keller C, Rando TA: Focal adhesion kinase signaling regulates the expression of caveolin 3 and beta1 integrin, genes essential for normal myoblast fusion. *Mol Biol Cell* 20: 3422–3435, 2009
69. Diaferia GR, Jimenez-Caliani AJ, Ranjitkar P, Yang W, Hardiman G, Rhodes CJ, et al.: β1 integrin is a crucial regulator of pancreatic β-cell expansion. *Development* 140: 3360–3372, 2013
70. Suleiman H, Zhang L, Roth R, Heuser JE, Miner JH, Shaw AS, et al.: Nanoscale protein architecture of the kidney glomerular basement membrane. *eLife* 2: e01149, 2013
71. Abrahamson DR: Role of the podocyte (and glomerular endothelium) in building the GBM. *Semin Nephrol* 32: 342–349, 2012
72. Potter AS, Drake K, Brunskill EW, Potter SS: A bigenic mouse model of FSGS reveals perturbed pathways in podocytes, mesangial cells and endothelial cells. *PLoS One* 14: e0216261, 2019
73. Bukosza EN, Kratochwill K, Kornauth C, Schachner H, Aufricht C, Gebeshuber CA: Podocyte RNA sequencing reveals Wnt- and ECM-associated genes as central in FSGS. *PLoS One* 15: e0231898, 2020
74. Rinschen MM, Gödel M, Grahammer F, Zschiedrich S, Helmstädter M, Kretz O, et al.: A multi-layered quantitative in vivo expression atlas of the podocyte unravels kidney disease candidate genes. *Cell Rep* 23: 2495–2508, 2018
75. Schell C, Sabass B, Helmstaedter M, Geist F, Abed A, Yasuda-Yamahara M, et al.: ARP3 controls the podocyte architecture at the kidney filtration barrier. *Dev Cell* 47: 741–757.e8, 2018
76. Wu C, Asokan SB, Berginski ME, Haynes EM, Sharpless NE, Griffith JD, et al.: Arp2/3 is critical for lamellipodia and response to extracellular matrix cues but is dispensable for chemotaxis. *Cell* 148: 973–987, 2012
77. Dhanda AS, Vogl AW, Albraiki SE, Otey CA, Beck MR, Guttman JA: Palladin compensates for the Arp2/3 complex and supports actin structures during *Listeria* infections. *MBio* 9: e02259-17, 2018
78. Taha M, Aldirawi M, März S, Seebach J, Odenthal-Schnittler M, Bondareva O, et al.: EPLIN-α and -β isoforms modulate endothelial cell dynamics through a spatiotemporally differentiated interaction with actin. *Cell Rep* 29: 1010–1026.e6, 2019
79. Dlugos CP, Picciotto C, Lepa C, Krakow M, Stöber A, Eddy M-L, et al.: Nephrin signaling results in integrin β1 activation. *J Am Soc Nephrol* 30: 1006–1019, 2019
80. Verma R, Venkatareddy M, Kalinowski A, Patel SR, Garg P: Integrin ligation results in nephrin tyrosine phosphorylation in vitro. *PLoS One* 11: e0148906, 2016
81. New LA, Keyvani Chahi A, Jones N: Direct regulation of nephrin tyrosine phosphorylation by Nck adaptor proteins. *J Biol Chem* 288: 1500–1510, 2013
82. Martin CE, New LA, Phippen NJ, Keyvani Chahi A, Mitro AE, Takano T, et al.: Multivalent nephrin-Nck interactions define a threshold for clustering and tyrosine-dependent nephrin endocytosis. *J Cell Sci* 133: jcs236877, 2020
83. Lussier G, Larose L: A casein kinase I activity is constitutively associated with Nck. *J Biol Chem* 272: 2688–2694, 1997

AFFILIATIONS

[1]Department of Molecular and Cellular Biology, University of Guelph, Guelph, Ontario, Canada
[2]Lunenfeld-Tanenbaum Research Institute, Sinai Health System, Toronto, Ontario, Canada
[3]Department of Biochemistry and Biomedical Sciences, McMaster University, Hamilton, Ontario, Canada
[4]Division of Oncology, Centre de Recherche du Centre Hospitalier Universitaire de Quebec–Laval University, Quebec City, Quebec, Canada
[5]Centre de Recherche sur le Cancer de l'Université Laval, Quebec City, Quebec, Canada
[6]Department of Human Health and Nutritional Science, University of Guelph, Guelph, Ontario, Canada
[7]Department of Cell and Developmental Biology, State University of New York Upstate Medical University, Syracuse, New York
[8]PROTEO–Quebec Network for Research on Protein Function, Engineering, and Applications Department of Molecular Biology, Medical Biochemistry and Pathology, Laval University, Quebec City, Quebec, Canada
[9]Department of Molecular Genetics, University of Toronto, Toronto, Ontario, Canada

Martin et al. Supplemental Material

Supplemental Video. Focal adhesions are less dynamic in Nck1/Nck2 double knockout podocytes.

Supplementa1 Table 1: Antibody information for immunoprecipitation experiments.

Supplemental Table 2: Antibody information for immunoblotting experiments.

Supplemental Table 3: Antibody information for immunofluorescent experiments.

Supplemental Table 4: Sequences used for CRISPR-Cas9 gene editing and TIDE analysis.

Supplemental Table 5: Primers used for semi-quantitative real-time reverse transcriptase polymerase chain reaction.

Supplemental Table 6: Primers used for genotyping.

Supplemental Figure 1. Generation of wildtype and Nck1 and Nck2 double knockout mouse podocyte cell lines.

Supplemental Figure 2. Gene expression analysis of wildtype and Nck1 and Nck2 double knockout podocytes.

Supplemental Figure 3. Normalized enrichment scores from gene set enrichment analysis of microarray data.

Supplemental Figure 4. Multi-faceted contributions of Nck1 and Nck2 to α actinin-4 and ß1 integrin-related cell adhesion.

Supplemental Figure 5. Loss of Nck1 or Nck2 (but not Nck1/2 haploinsufficiency) results in biochemical abnormalities and susceptibility to disease.

Supplemental References

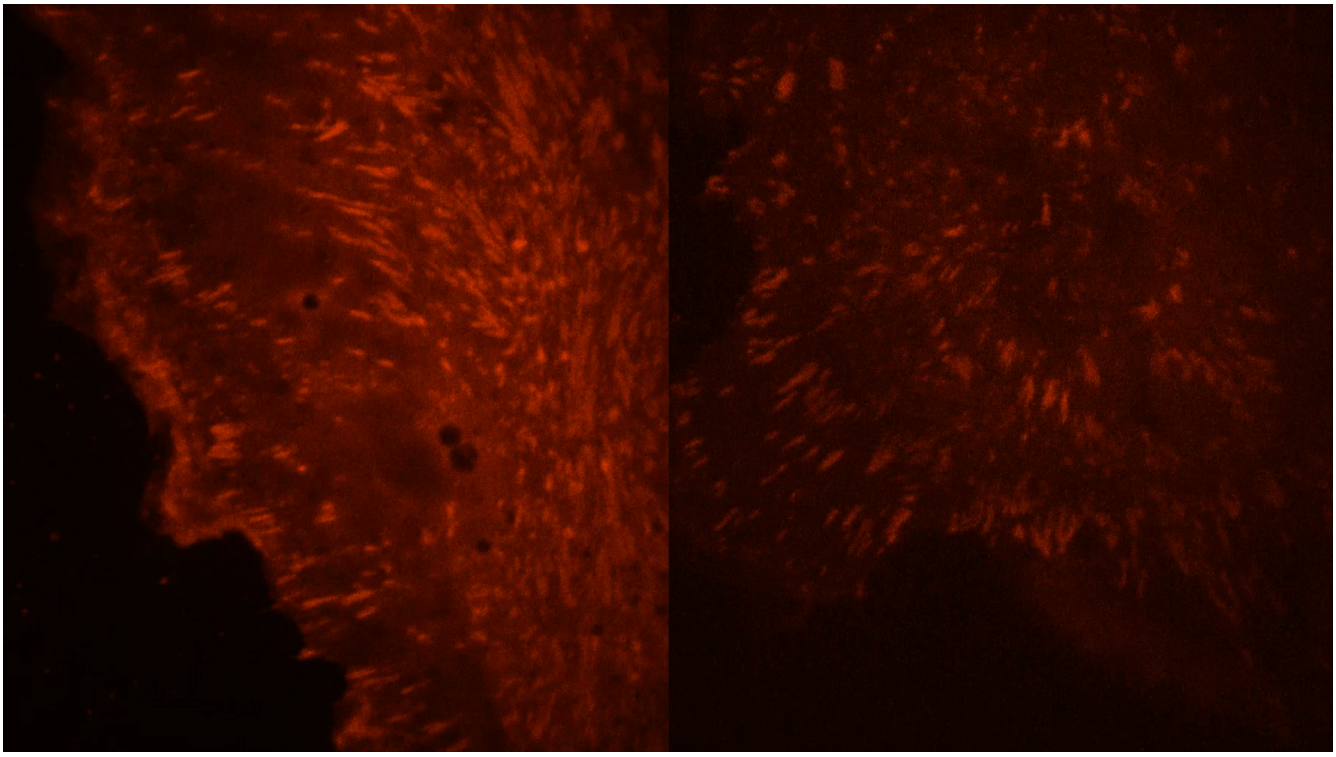

Supplemental Video. Focal adhesions are less dynamic in Nck1/Nck2 double knockout podocytes. Wildtype (left) and Nck1/2 double knockout (right) podocytes were transduced with paxillin-mCherry adenovirus. Images were taken each minute for 22 minutes to profile focal adhesion dynamics. 100x optical zoom. Video file available online in Supplemental Material section.

Supplemental Table 1: Antibody information for immunoprecipitation experiments. Pr-A: proteinA-sepharose beads.

Immunoprecipitation			
Antibody	Species	Source	Concentration
anti–IgG	rabbit	Cell signalling; 2729	1ul/ 100ul Pr-A beads
anti–Nck (1794)	rabbit	Larose Lab[83]	1ul/ 100ul Pr-A beads
anti–α actinin 4	rabbit	Abcam; ab108198	1ul/ 100ul Pr-A beads
Magnetic anti–FLAG beads	mouse	Sigma; M8823	20 μL of a 50% magnetic anti-FLAG M2 beads/ IP

Supplemental Table 2: Antibody information for immunoblotting experiments.

Western Immunoblotting			
Antibody	Species	Source	Concentration
anti–GAPDH	mouse	Applied Biologic Materials Inc.; G041	1:1000
anti–*β*-actin	mouse	Sigma-Aldrich; A5441	1:2000
anti–Nck (1794)	rabbit	Larose Lab[83]	1:1000
anti–mouse HRP	goat	Bio-Rad; 170–6516	1:10000
anti–rabbit HRP	goat	Bio-Rad; 170–6515	1:10000
anti–FLAG M2	mouse	Sigma-Aldrich; F3165	1:2000
anti–WT-1 (C-19)	rabbit	Santa Cruz; sc-192	1:500
anti–eplin	rabbit	Thermo Proteintech; 16639-1-AP	1:2000
anti–palladin	rabbit	Thermo Proteintech; 10853-1-AP	1:2000
anti–p130-Cas	mouse	BD Biosciences; 610272	1:1000
anti–Fak	rabbit	Millipore; 04-591	1:1000
anti–actin	rabbit	Cytoskeleton; AAN01	1:500
anti– *β*1 integrin	mouse	Santa Cruz; sc-9970	1:1000
anti–Nck	mouse	BD Biosciences; N15920	1:1000
anti– α actinin-4	rabbit	Abcam; ab108198	1:2000

Supplemental Table 3: Antibody information for immunofluorescent experiments.

Immunofluorescence			
Antibody	Species	Source	Concentration
anti–nephrin	guinea pig	20R-NP002; Fitzgerald Inc.	1:100
anti–synaptopodin	mouse	Fitzgerald; 10R-2373	1:150
anti–WT-1	rabbit	Santa Cruz; sc-192)	1:50
anti–paxillin	rabbit	Santa Cruz; sc-5574	1:50
anti–paxillin	rabbit	Abcam; Ab32054	1:100
anti–paxillin 5H-11	mouse	Upstate; 05-417	1:100
anti–β1 integrin	rat	Millipore; MAB1997	1:500
anti–active β1 integrin	rat	BD Biosciences; BD550531	1:50
anti–laminin a5	mouse	DSHB P3H9	neat
TexasRed phalloidin	-	T7471; Invitrogen	1:50
Phalloidin-647	-	A30107; Invitrogen	1:100
anti–Alpha actinin-4	rabbit	Abcam; ab108198	1:100
anti–FLAG-M2	mouse	Sigma; F3165	1:100
anti–rabbit Alexa Fluor 488	goat	A11008; Invitrogen	1:400
anti–rabbit Alexa Fluor 594	goat	A11076; Invitrogen	1:400
anti–mouse Alexa Fluor 488	goat	A11001; Invitrogen	1:400
anti–mouse Alexa Fluor 594	goat	A11005; Invitrogen	1:400
anti–rat Alexa Fluor 488	goat	A11006; Invitrogen	1:400
anti–guinea pig Alexa Fluor 594	goat	A11076; Invitrogen	1:400

Supplemental Table 4: Sequences used for CRISPR-Cas9 gene editing and TIDE analysis. FW, forward; RV, reverse.

Gene Target	Guide Sequence (FW/RV)	TIDE Primer (FW/RV)	TIDE Efficiency
Actn4	TACCAGTACGGCCCGAACAG	AGTTCCATTGCAACCTCCCG	93.9%
	CTGTTCGGGCCGTACTGGTAC	CATTCATGACTTGGGCCCCG	
Palld	ACGGAAGCTTCGCTTCAAGG	TGCCATCAGTACTTCCGTGT	90.9%
	CCTTGAAGCGAAGCTTCCGTC	CCCTATGGGTGTCCGAACCT	
Lima1	TCGTGGCTGTTCTCTGAGCG	n/a	undetermined
	CGCTCAGAGAACAGCCACGAC	n/a	

Supplemental Table 5: Primers used for semi-quantitative real-time reverse transcriptase polymerase chain reaction. FW, forward; RV, reverse.

Gene target	Primer (FW/RV)	Harvard primer bank number
Gapdh	AGGTCGGTGTGAACGGATTT	
	GGGGTCGTTGATGGCAACA	
Hprt	CATGGACTGATTATGGACAGG	
	ATCCAGCAGGTCAGCAAAGAA	
Nck1	GCGGTCCTCAGGTGACTGG	
	ATTCATGGAATTTCGAACTCGCCAC	
Nck2	AGGACAGGCTACGTGCCTT	
	GTACTCCGCATCAGTGCTTGG	
Mmp2	CAAGTTCCCCGGCGATGTC	6678902a1
	TTCTGGTCAAGGTCACCTGTC	
Mmp13	CTTCTTCTTGTTGAGCTGGACTC	6678896a1
	CTGTGGAGGTCACTGTAGACT	
Intav	GGGCCTATTGTTCAGCACAT	
	GATTCCACAGCCCAAAGTGT	
Intb3	GTAATCGAGATGCCCCAGAG	
	CTTCCATCCAGGGCAATATG	
Inta3	TGCCGTTCTAAATCCTCCAC	
	CACCGGTAGTCAGGCAATTT	
Intb1	GGTGTCGTGTTTGTGAATGC	
	TCCTGTGCACACGTGTCTT	
Lama5	ACCCAAGGACCCACCTGTAG	
	TCATGTGTGCGTAGCCTCTC	
Lamb2	CGTGACCATCCAACTGGACCTGG	
	CCAAGCCTTCCCAAAGTCAGAAG	
Col4a1	CTGGCACAAAAGGGACGAG	33859528a1
	ACGTGGCCGAGAATTTCACC	
Col4a2	GACCGAGTGCGGTTCAAAG	556299a1
	CGCAGGGCACATCCAACTT	
Col4a3	CAAAGGCATCAGGGGAATAACT	6680968a1
	ATCCGTTGCATCCTGGTAAAC	
Col4a4	ATGAGGTGCTTTTTCAGATGGAC	34328045a1
	GGGGCCGCCATACTTCTTG	
Col4a5	AGGCGAAATGGGTATGATGGG	26348681a1
	CTCCCTTACCGCCCTTTTCTC	
Col5a2	CCCTGGCTTGAAAGGTCACAG	86613789c3
	GCCCATAGCACCCATTGGAC	
Col1a1	TAAGGGTACCGCTGGAGAAC	
	GTTCACCTCTCTCACCAGCA	
Fn1	ATGTGGACCCCTCCTGATAGT	
	GCCCAGTGATTTCAGCAAAGG	

Supplemental Table 6: Primers used for genotyping. FW, forward; RV, reverse; Podo-dKO, podocyte-specific Nck1/Nck2 double knockout; KO, knockout.

Gene target	Primer (FW/RV)	Mouse line
Cre	GCAGAACCTGAAGATGTTCGC	Podo-dKO
	GCACGTTCACCGGCATCAACG	
Rtta	CGCACTTCAGTTACTTCAGGTCCTC	Podo-dKO
	GCTTATGCCTGATGTTGATGATGC	
Nck1 WT	GCATGTAGACAATTACACTTCAGCACC	Podo-dKO Nck1KO
	ATTCATGGAATTTCGAACTCGCCACC	
Nck1 lacZ	CTGATTGAAGCAGAAGCCTGCGATG	Podo-dKO Nck1KO
	TATTGGCTTCATCCACCACATACAGG	
Nck2 flox	GGATACCACATTGGCATTAGTAG	Podo-dKO
	GTGCTCATTTGACAAGTGACAC	
Nck2KO WT	CTACACTGCCCAGCAGGACCAGG	Nck2KO
	CACATACAGATACACACACGCTGAAG	
Nck2KO KO	CCAATGGCAAAGGTGATCATGACGG	Nck2KO
	CGCCTTCTATCGCCTTCTTGACGAG	

Supplementary figure 1

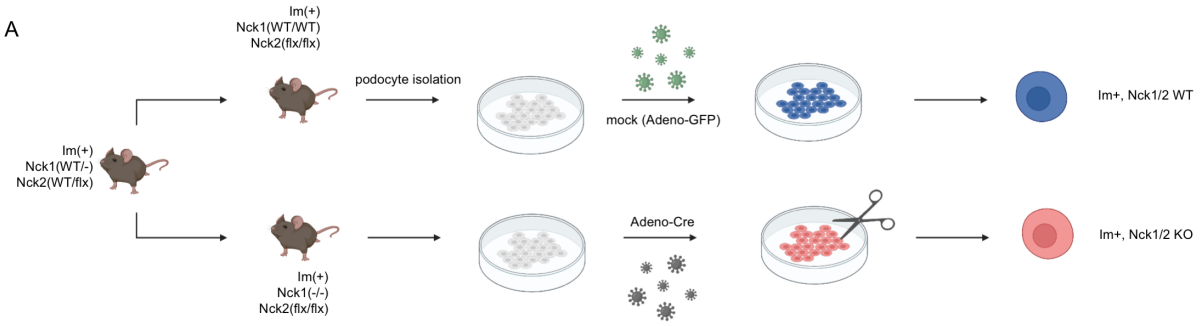

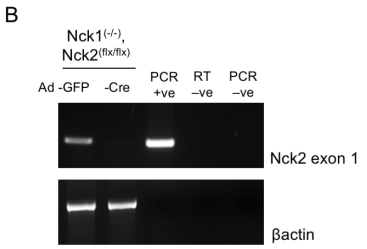

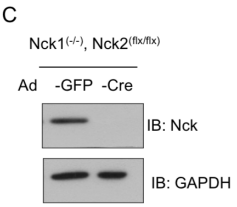

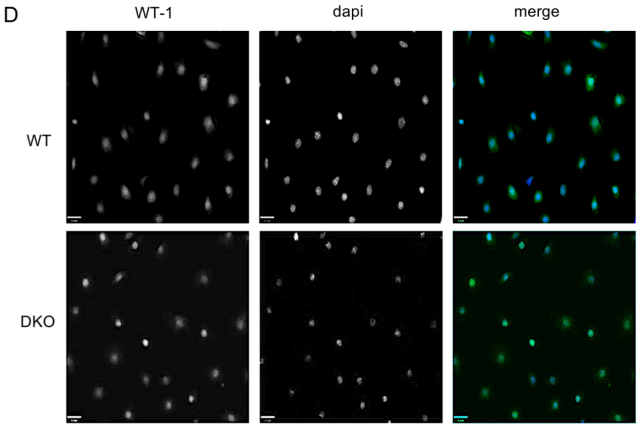

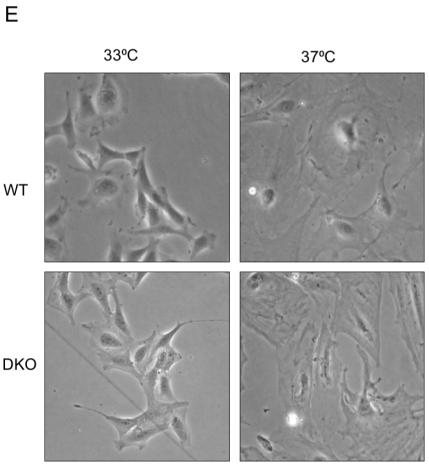

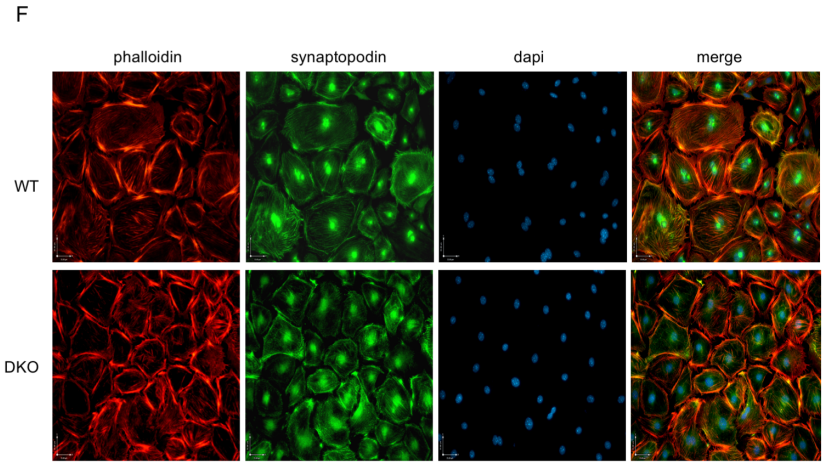

Supplemental Figure 1. Generation of wildtype and Nck1 and Nck2 double knockout mouse podocyte cell lines. (A) Scheme for generation of wildtype (WT) and Nck1 and Nck2 double knockout (dKO) conditionally immortalized mouse podocyte cell lines (MPCs). (B) Reverse transcriptase polymerase chain reaction (RT PCR) demonstrating adenoviral expression of Cre (adeno-Cre) but not mock (adeno-GFP) allows for targeted excision of floxed Nck2 and the generation of dKO cells. (C) Western immunoblot (IB) validating knockout of Nck1 and Nck2 in podocyte cell lines. (D) Immunofluorescent (IF) imaging of Wilm's Tumour (WT)-1 in WT and dKO podocytes. (E) Phase-contrast images of WT and dKO MPCs cultured under permissive (33ºC, IFNγ supplementation) and differentiating (37ºC) conditions. (F) IF imaging of phalloidin and synaptopodin in WT and dKO MPCs.

Supplementary figure 2

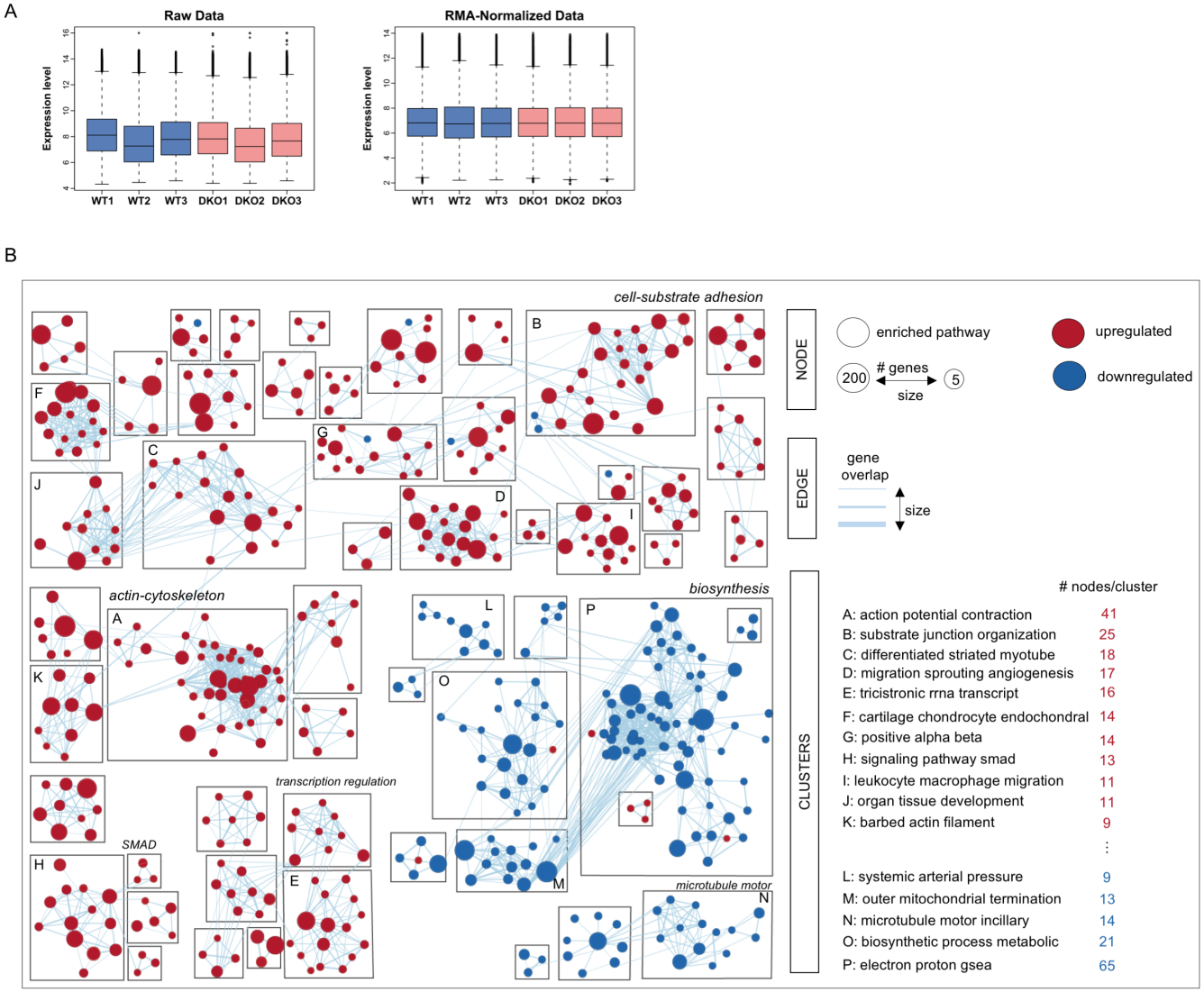

Supplemental Figure 2. Gene expression analysis of wildtype and Nck1 and Nck2 double knockout podocytes. (A) BoxPlots of raw and RMA-normalized microarray data from 3 biological replicates. (B) Gene set enrichment analysis (GSEA) map generated from microarray of WT and dKO MPCs (FDR *Q* value < 0.05 and combined coefficient >0.375 with combined constant = 0.5). Red and blue nodes represent up- and down-regulated genes respectively. Node size is proportional to the number of genes per term. Node clusters were labelled using AutoAnnotate following manual organization in Cytoscape. Labels for minimally interconnected networks were removed for clarity.

Supplementary figure 3

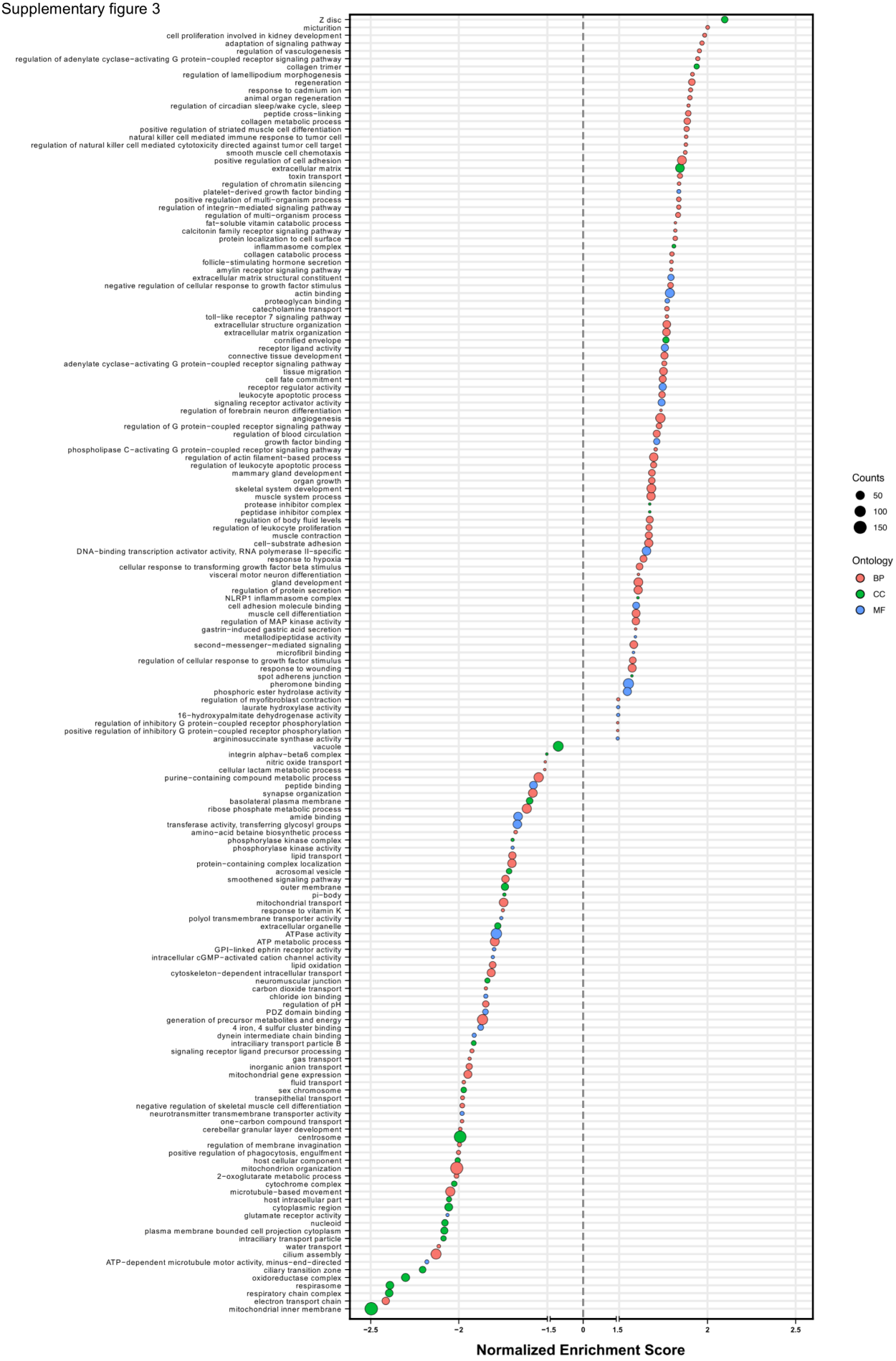

Supplemental Figure 3. Normalized enrichment scores from gene set enrichment analysis of microarray data. (A) Dot plot of normalized enrichment scores for terms in upregulated and downregulated gene sets generated from gene set enrichment analysis of microarray data. Enriched gene ontology terms (Biological process (BP), Cell component (CC) and Molecular Function (MF)) are represented by dot colour and the relative abundance of genes (counts)/ term is indicated by dot size.

Supplementary figure 4

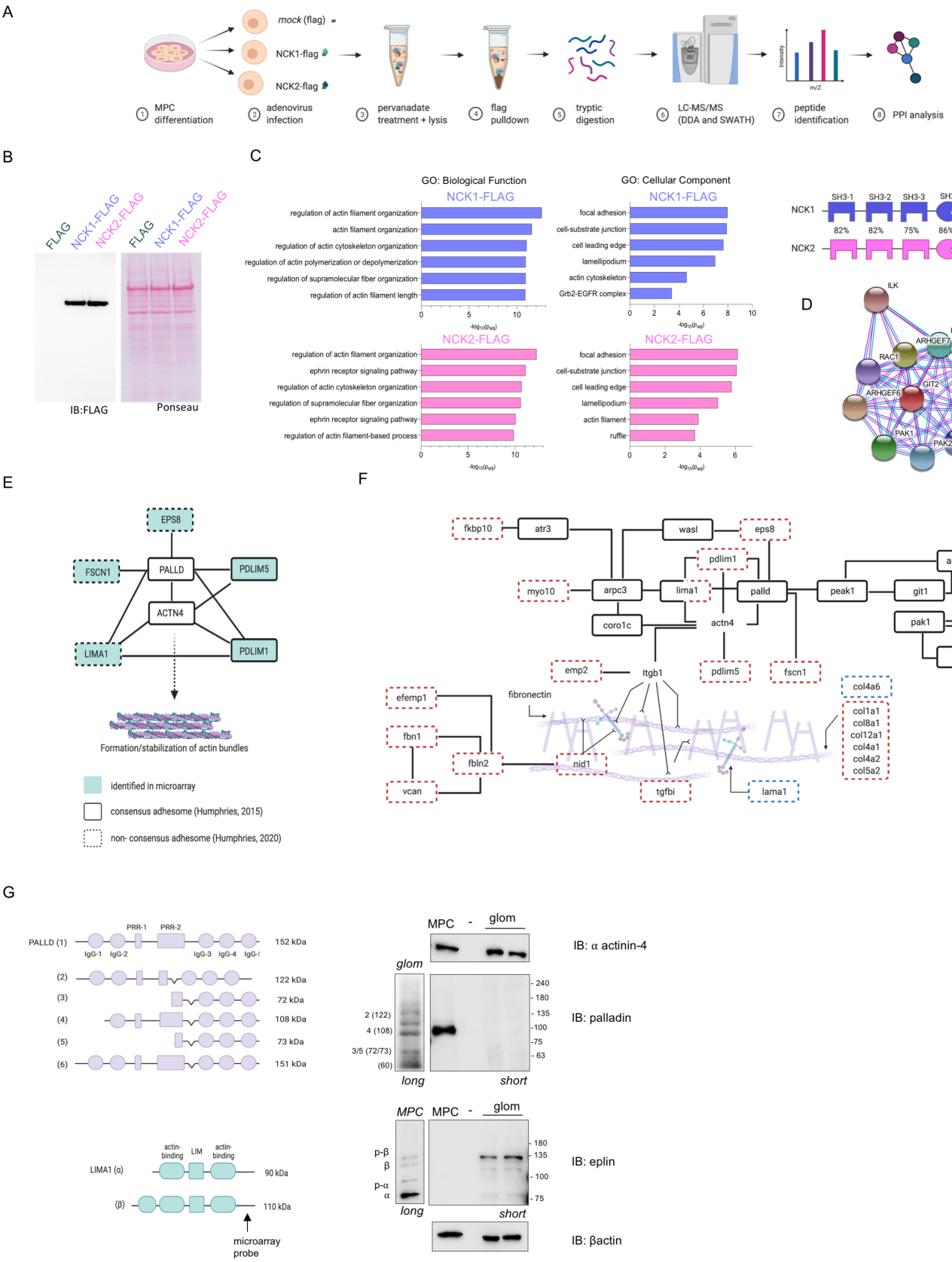

Supplemental Figure 4. Multi-faceted contributions of Nck1 and Nck2 to α actinin-4 and ß1 integrin-related cell adhesion. (A) Experimental workflow for affinity purified mass spectrometry (AP-MS)-based identification of NCK1 and NCK2 protein interactors in mouse podocyte cells (MPCs). FLAG-NCK1, FLAG-NCK2 or FLAG (control) 'baits' were delivered using adenovirus in differentiated WT podocytes and subsequently affinity purified alongside interacting 'prey' proteins from cell lysates (B) Ponceau staining and flag immunoblot (IB) of samples used for AP-MS. (C) Gene ontology (GO) analysis of biological function and cellular componentry of preys captured by NCK1 or NCK2 and identified by AP-MS. NCK1 and NCK2 binding domain homology is high, as is the similarity of the enrichment terms identified. (D) String enrichment of ßPix, GIT, PAK and Nck. (E) Relationship between α actinin-4 binding partners (as identified by string) that were also identified as upregulated genes in Nck1 and 2 double knockout (dKO) cells by microarray. (F) Established interactions (identified by string) between NCK1 and NCK2 interactors identified by AP-MS and genes >2-fold mis-regulated by microarray that are relevant to α actinin-4 and ß1 integrin-related cell adhesion. Red boxes indicate upregulated genes while blue boxes represent downregulated genes. (G) Isoform structure and protein expression profiles of eplin and palladin in MPCs and mouse glomerular samples. Palladin expression was restricted to a ~108 kDa isoform in wildtype podocyte cells. Conversely, several palladin isoforms could be detected in mouse glomerular samples, albeit in low abundance compared to cultured cells. On the contrary, eplin was highly expressed in glomerular samples and a band likely corresponding to the ß isoform was enriched, while expression of a band corresponding to the presumed α isoform was predominant in cultured podocytes. Interestingly, in cells exposed to shear stress, eplin's ß isoform predominates and functions in actin bundle stabilization[84]. Conversely, eplin's α isoform is more widely expressed and contributes to actin dynamics through its inhibition of Arp2/3 actin branching downstream of WASp/WAVE. Doublets of each eplin isoform were observed, the possible result of phosphorylation events, which increase eplin's affinity for actin[85].

Supplementary figure 5

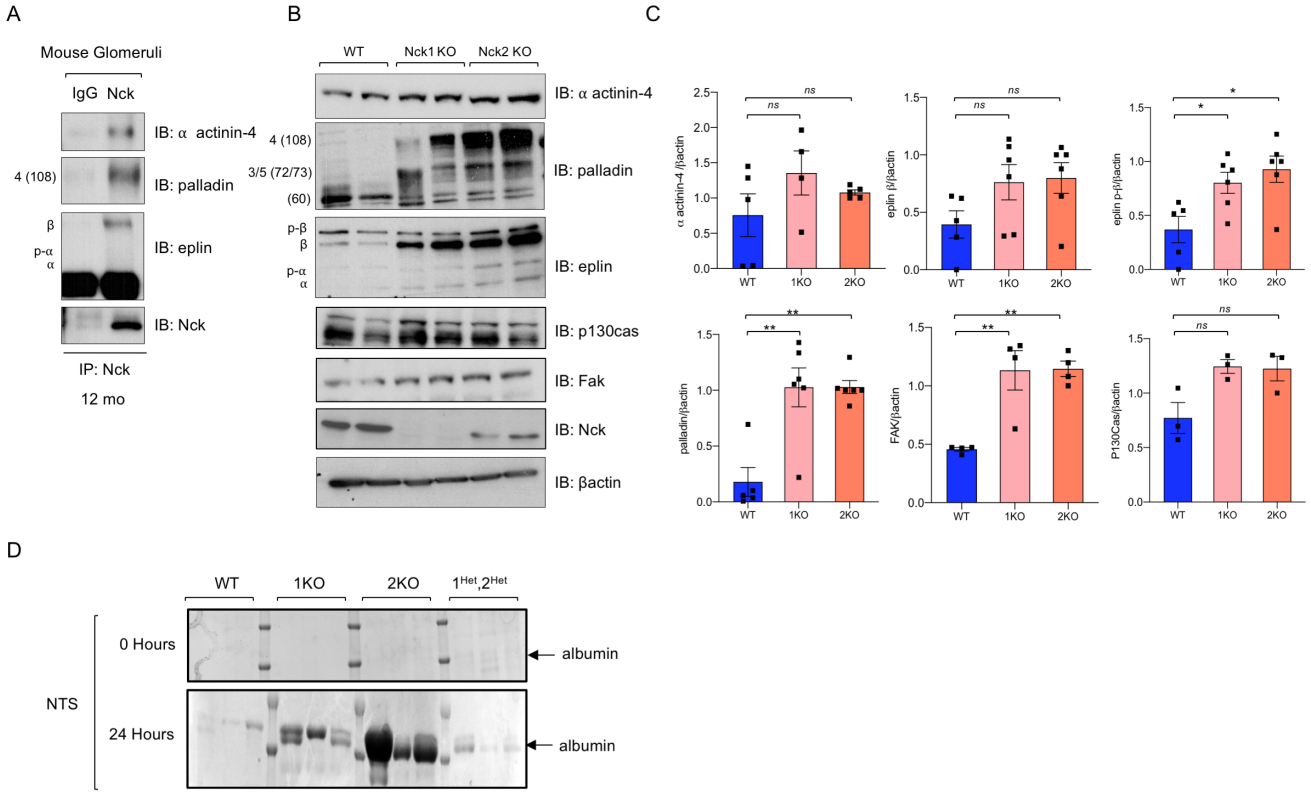

Supplemental Figure 5. Loss of Nck1 or Nck2 (but not Nck1/2 haploinsufficiency) results in biochemical abnormalities and susceptibility to disease. (A) Co-immunoprecipitation (IP) of Nck with α actinin-4, palladin and eplin from glomerular lysates of wildtype (WT) mice. (B) Immunoblotting (IB) and densitometric quantification (C) of glomerular lysates from wildtype (WT), Nck1 knockout (Nck1KO) and Nck2KO mice at 8 weeks of age. (C) Coomassie urine gel of WT, Nck1KO, Nck2KO, and Nck1-/+, Nck2-/+ (double heterozygous) at the peak timepoint (24 hours) of nephrotoxic serum (NTS) induced-disease.

Supplemental References

83. Lussier G, Larose L: A casein kinase I activity is constitutively associated with Nck. *J. Biol. Chem.* 272: 2688–2694, 1997

84. Maul RS, Song Y, Amann KJ, Gerbin SC, Pollard TD, Chang DD: EPLIN regulates actin dynamics by cross-linking and stabilizing filaments. *J. Cell Biol.* 160: 399–407, 2003

85. Han M-Y, Kosako H, Watanabe T, Hattori S: Extracellular signal-regulated kinase/mitogen-activated protein kinase regulates actin organization and cell motility by phosphorylating the actin cross-linking protein EPLIN. *Mol. Cell. Biol.* 27: 8190–8204, 2007